Journal of Mining and Environment (JME) Vol. 18, No. 4, 2026, 1343-1369

Shahrood University of Technology

Journal of Mining and Environment (JME)

Journal homepage: www.jme.shahroodut.ac.ir

Iranian Society of Mining Engineering (IRSME)

Exploring Crack Growth Patterns of Anisotropic Materials in Bi-Material Notched Discs: Insights from a Combined Experimental and Numerical Approach

Vahab Sarfarazi[1], Hadi Haeri[2*], Jinwei Fu[3], Shadman Mohammadi[1], and Alireza Shaker[4]

1.Department of Mining Engineering, Hamedan University of Technology, Hamedan, Iran,
2.Department of Mining Engineering, Higher Education Complex of Zarand, Shahid Bahonar University of Kerman, Kerman, Iran,
3.School of Civil Engineering and Transportation, North China University of Water Resources and Electric Power, Zhengzhou, 450046, China,
4.Department of Geology, Faculty of Sciences, Shahid Bahonar University of Kerman, Kerman, Iran

Article Info

Received 22 December 2025
Received in Revised form 2 April 2026
Accepted 26 July 2026
Published online 26 July 2026

DOI: 10.22044/jme.2026.17350.3438

Keywords

Anisotropy
Tensile crack
Notch
PFC

Abstract

In this research, samples of bi-material notch discs were created and examined in the laboratory to investigate their mechanisms of indirect tensile failure. Brazilian tensile strength tests were conducted to determine the mechanical properties of these samples under a loading rate of 0.016 mm/s. The discs were designed with a central notch and were made from two materials: concrete and gypsum. Gypsum (Material 1) was placed at the center (core), while concrete (Material 2) was used to form a peripheral strip (ring) around this core. The core diameter and ring thickness were varied, resulting in a total of 21 specimens that were prepared and subjected to axial loading during testing. To support the experimental results, the Particle Flow Code (PFC) was utilized to simulate the tests. It was observed that both the notch dimensions and the choice of materials significantly influenced the mechanical behavior and fracture characteristics of anisotropic rocks. Furthermore, based on the results obtained from the laboratory samples and the modeling of these samples using PFC software, strong agreement was achieved regarding crack growth behavior. In addition, a comprehensive study was conducted on the samples through numerical modeling, which included the distribution of bond forces and Rosette diagrams, as well as crack growth patterns.

1. Introduction

The rock masses are mainly accompanied by joints, fractures, bedding planes, and other defects. These discontinuities exist in engineered rock structures, such as surface and underground mines, rock slopes, and tunnels. They cause changes in mechanical behavior and reduce the strength parameters. The stability, safety, and useful life period of these structures are of the utmost importance to design engineers [1, 2]. Researchers have conducted numerous studies on the strength and stability parameters of rock samples, including those with weak cement and cemented rock blocks at the rock mass scale [3-9]. The micro-defects are considered to produce the weak planes in the rock masses and increase the degree of anisotropy in the structures during the working period. They dramatically affect the strength and failure processes in the jointed rocks compared to those of the intact rock materials. In recent decades, the development of huge mining and civil engineering projects on both the surface and underground has motivated many investigators to struggle for the accurate measurement, computation, and estimation of the rocks' strength parameters through laboratory tests, field measurements, numerical simulations, and data processing approaches [3, 10]. Most of these researchers developed new methods and conducted experimental and numerical studies to depict the influence of discontinuities and defects on the mechanical characteristics and failure strength of rock masses under various loading environments

Corresponding author: hadihaeri@uk.ac.ir (H. Haeri)

by considering isotropic, anisotropic, homogeneous and nonhomogeneous circumstances [11, 12]. However, due to various engineering applications and the complexity of the rock mass conditions in these projects, the challenges for conducting laboratory and large-scale in situ tests on the defected rocks and rock material specimens and simulating them with sophisticated numerical soft wares are still under way and continued [4]. The laboratory tests for measuring the mechanical characteristics and failure strength modes of intact rock samples are relatively straightforward. However, the improvements in technology and the need for more delicate and precise engineering applications of rock material, as well as the need for calibration and verification of the laboratory tests and numerical methods, sometimes necessitate the tests on intact rock samples as well. On the other hand, it has been proved that the accuracies of the laboratory tests' results on relatively small scales are mostly insufficient for many delicate engineering applications and that large-scale in situ tests are impossible for many rock masses [6]. The RMR (rock mass rating), Q, and GSI (geological strength index) systems of rock mass classifications are the most commonly used empirical approaches for estimating the mechanical characteristics of rocks in many engineering projects [13-16]. However, many complex features of discontinuities such as density, roughness, direction, filling conditions, degree of alterations, scale, etc. are not considered specifically in these rating systems of rock masses [17]. Many researchers stated that these systems are case sensitive, conservative and uncertain for many delicate and important engineering projects [18-20]. The tensile strengths of anisotropic layered rocks were considered by some researchers who investigated the relations between five elastic parameters of these transversely isotropic rocks and their tensile strengths [21, 22]. Lab-scale investigations and numerical simulations have been conducted on the measurement and analysis of fracture toughness and the crack propagation process in anisotropic rock specimens. The tensile strength, shear failure, and mechanical behavior of anisotropic and heterogeneous rocks containing pre-existing cracks with different inclination angles (related to the loading direction) were discussed [19, 21, 22]. In some recent studies, Haeri et al. [23, 24] studied the effects of double and multiple cracks within the disc type rock specimens on the failure mechanism and strengths of rocks under compression. They found that the wing cracks were induced and propagated in the disc in the direction of the compressive applied load. The mechanical behavior and tensile failure mode of anisotropic shale specimens were studied by Tan et al. [25]. They carried out a detailed study utilizing both experimental and numerical methods to examine the significant effects of anisotropy on rock samples. Their findings revealed substantial impacts on various parameters, including crack initiation and growth, bearing capacity, and the distribution of induced stresses within the samples. The sophisticated numerical models were developed in relatively recent years for the numerical simulation of mechanical characteristics and fracturing mechanisms of rock masses. The discrete element method (DEM) has been enhanced by many researchers for efficient simulation of geo-materials, enabling the study of their mechanical behaviors and failure modes in various loading environments [26-40]. The rock mass samples are treated as assemblies of individual solid particles that move relative to one another. During the loading process, there are some interactions between the particles and defects within the modelled specimens. The numerical formulation of the geo-material samples is explicitly developed, while in its counterparts (the finite element method (FEM), an equivalent implicit formulation is developed and the system of algebraic equations is solved implicitly [41]. The mechanical behavior of jointed rocks and the crack propagation mechanisms in rock materials considering the process of crack initiation, growth and coalescence have been investigated experimentally through laboratory tests and simulated numerically by DEM using PFC2D and PFC3D [42, 43]. For example, Sarfarazi et al. [44] accomplished some investigation into the failure mode and crack growth mechanism in geo-material specimens using PFC2D and PBM. On the other hand, there are some deficiencies in modeling the jointed fractured rocks by using only PBM. Therefore, the Flat-jointed model (FJM) is proposed to overcome these deficiencies and improve PFC2D for modelling fractured jointed rocks exhibiting anisotropy and non-homogeneity to the rock structures under various loading environments [45-48]. The novelty of this study lies in the combined experimental and numerical investigation of the fracture behavior of anisotropic bi-material notch discs under indirect tensile loading. The effects of notch geometry and material heterogeneity on crack initiation and propagation are examined, and the numerical modeling is performed using the PFC2D platform and the parallel-bonded model (PBM).

2. Experimental Program

2.1. Mix Proportions and Properties

To simulate the notched gypsum disc surrounded by a concrete mixture, the gypsum materials were blended well, with a weight ratio of 1.5 to 1 (gypsum to water). The plastic cylinder dimensions (diameter × height) were 12 cm × 8 cm. To create the notched gypsum core, a steel plate with a length of 2 cm was pre-inserted into the gypsum cylinder and removed after the initial hardening of the gypsum sample (Figure 1). Subsequently, the gypsum sample was placed inside a larger cylinder, and the concrete mixture was poured into the mold. To reduce the influence of measurement deviations and enhance data robustness, each testing scenario included three rock blocks with comparable pre-existing cracks. The gypsum diameters (D in Figure 2) were 3 cm, 6 cm, and 9 cm, and the concrete thicknesses (C in Figure 2) were 4.5 cm, 3 cm, and 1.5 cm. Bi-material disc samples containing one notch were constructed. The notch inclination (α in Figure 3) varied from 0° to 90° in 15° increments. Additionally, three intact samples were prepared (Figure 2). A total of 24 different models were tested under axial compressive loading. The curing process, which is crucial, was conducted for 28 days in a cool, well-ventilated environment (Figure 1g).

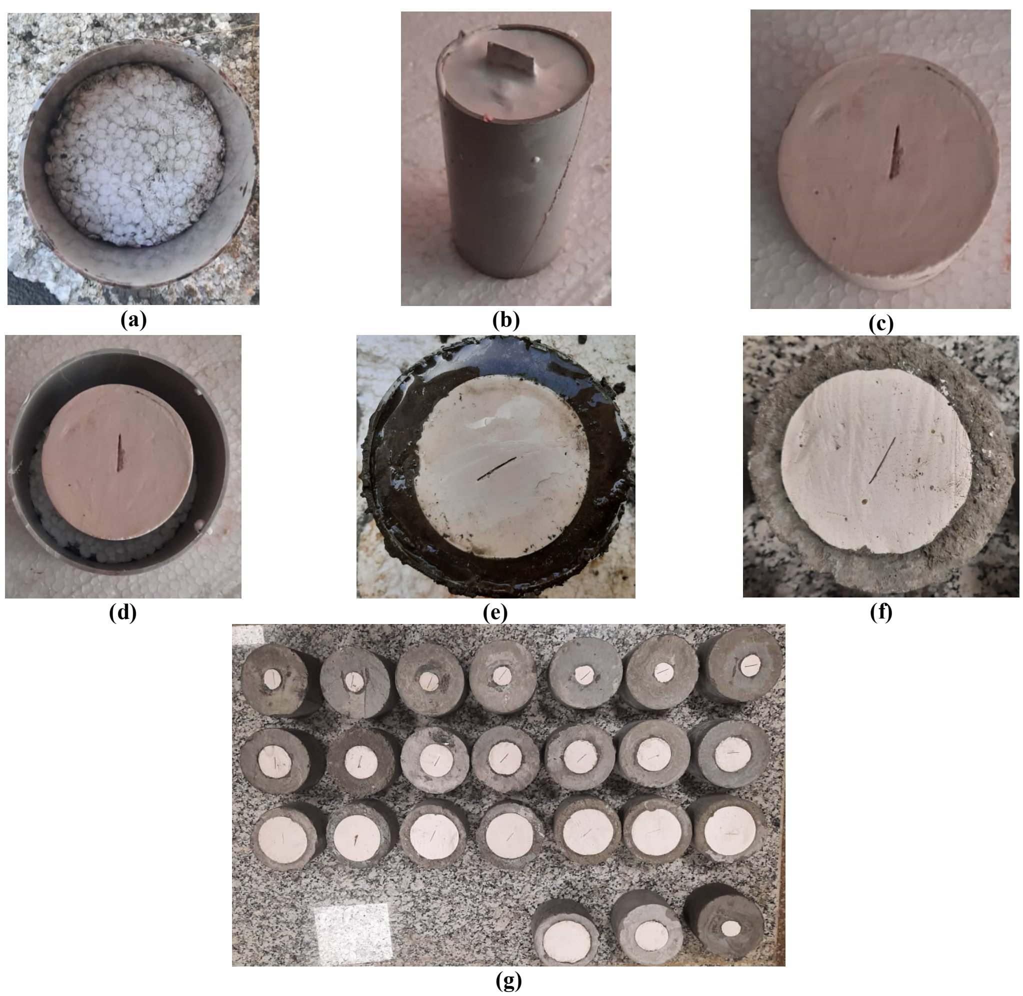

Figure 1. Sample preparation stages.

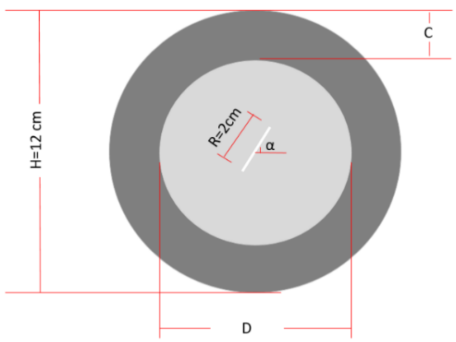

Figure 2. Schematic view of bi material disc sample containing a central notch.

The concrete mixture detailed in this article consists of 500 kg of cement, 25 kg of silica fume, 168 kg of water, 810 kg of fine aggregate, 810 kg of coarse aggregate, and 6.825 kg of superplasticizer. The mechanical properties of both gypsum and concrete samples, as determined by relevant tests, show that the indirect tensile strength of gypsum is 1 MPa, while concrete has an indirect tensile strength of 2.2 MPa. The compressive strength of concrete is significantly higher at 21 MPa compared to gypsum's compressive strength of 7.2 MPa. Furthermore, the Young's modulus of gypsum is 3 GPa, while concrete has a Young's modulus of 10 GPa. The Poisson's ratio for gypsum is 0.15, whereas for concrete it is 0.11.

2.2. Brazilian Loading Test

Brazilian tensile strength tests were conducted in the laboratory as shown in Figure 3. The apparatus used for these tests features a hydraulic pump with a maximum stroke of 150 mm and a capacity of 150 tons. Displacements (up to 400 mm) were measured using an LVDT mounted on the loading plate. The load cell has a capacity of 225 tons. The specimens were loaded at a constant load rate of 20 kN/min during the tests. Continuous records of the applied load and deflection were captured by a data logger. The tests were carried out up to approximately 85% of their maximum bearing load.

Figure 3. Axial loading test.

2.3. Characteristics of Crack Development in the Tested Disc-Shaped Specimens

Crack development was continuously documented during loading, and each disc specimen ultimately experienced tensile-dominated failure, as illustrated in Figures. 4–8. For notch angles exceeding 45°, tensile cracks initiated at the notch tips and propagated parallel to the loading axis until reaching the sample's boundary. Conversely, for notch angles less than 45°, cracks originated from the notch walls and propagated similarly within the geomaterial specimen. In the intact models, it was observed that tensile cracks primarily propagated at the interface between concrete and gypsum.

2.4. Tensile strength of experimental samples

Figures 9 and 10 illustrate the tensile strength of bi-material notched discs with various notch angle configurations. The data show that, for a fixed gypsum diameter, the tensile strength reaches its minimum at a notch angle of 30° and its maximum at 90°. Additionally, increasing the concrete thickness enhances the tensile strength of the notched specimen.

a) 90° b) 75° c) 60° d) 45°

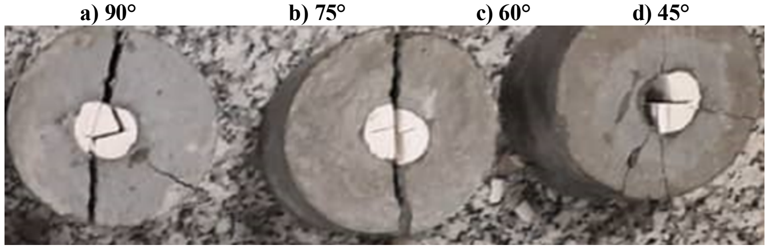

e) 30° f) 15° g) 0°

Figure 4. Failure pattern in experimental sample containing the central notch; gypsum diameter was 3cm.

a) 90° b) 75° c) 60° d) 45°

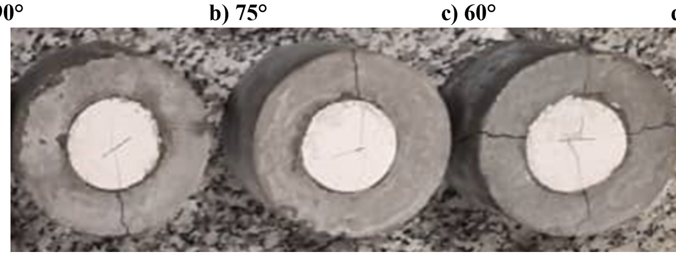

e) 30° f) 15° g) 0°

Figure 5. Failure pattern in experimental sample containing the central notch; gypsum diameter was 6cm.

a) 90° b) 75° c) 60° d) 45°

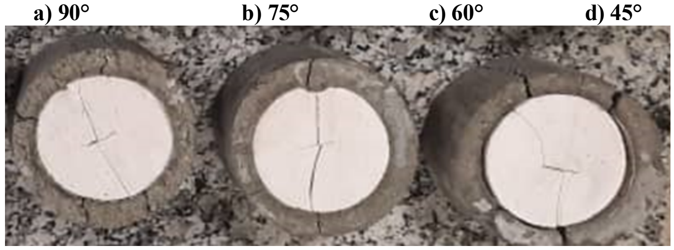

e) 30° f) 15° g) 0°

Figure 6. Failure pattern in experimental sample containing the central notch; gypsum diameter was 9cm.

a) 9cm b) 6cm c) 3cm

Figure 7. Failure pattern in experimental intact sample with different gypsum diameters.

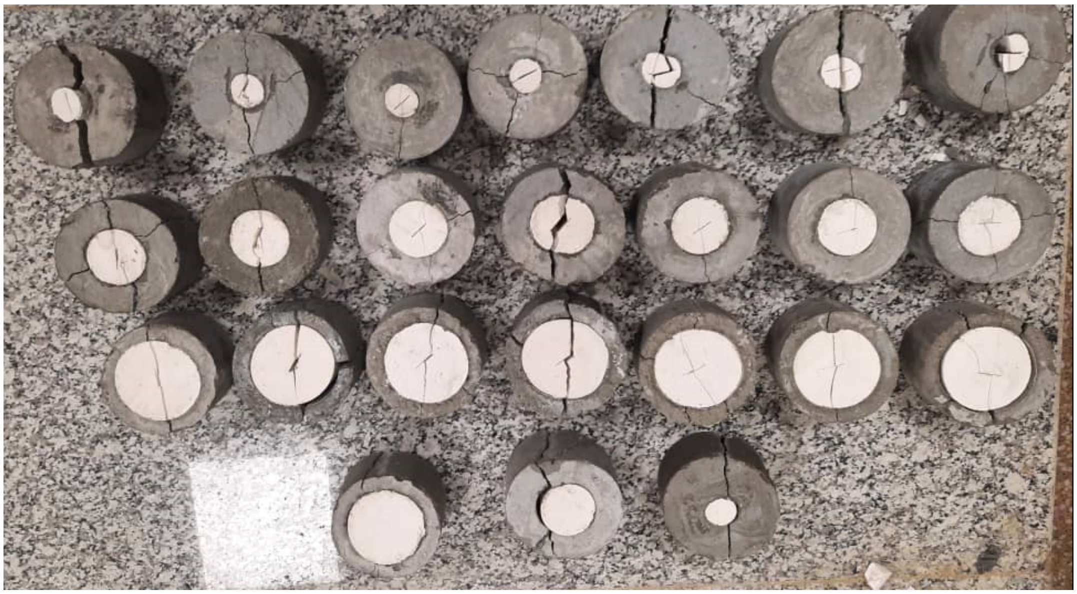

Figure 8. Failure pattern in all of the experimental samples.

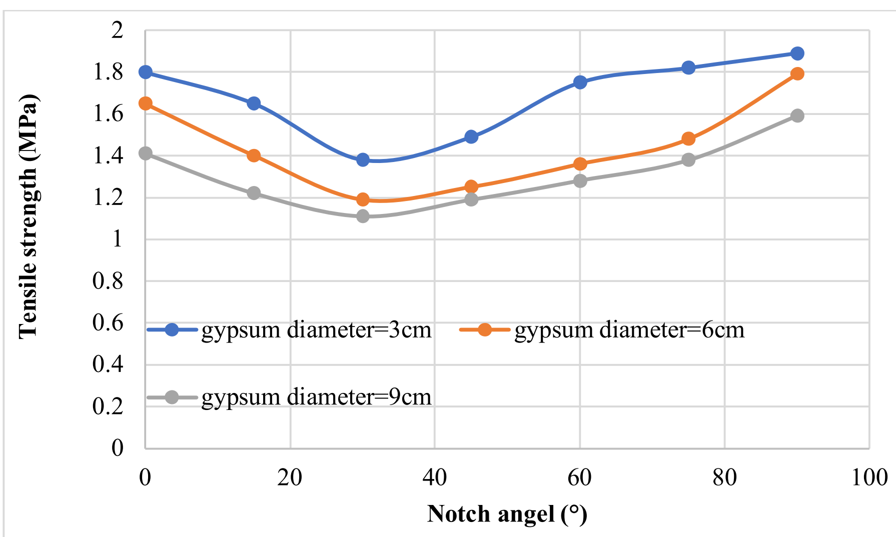

Figure 9. The variation of tensile strength versus notch angle for different gypsum diameter.

Figure 10 shows the tensile strength of intact bi-material discs with different gypsum diameters. Comparing Figure 9 and Figure 10, it can be concluded that when the gypsum diameter was 3 cm and the notch angle was 30°, the tensile strength was 15% less than that of the intact bi-material model, while at a notch angle of 90°, it was 2% less. When the gypsum diameter was 6 cm and the notch angle was 30°, the tensile strength was 26% less than that of the intact bi-material model, and at 90°, it was 7% less. When the gypsum diameter was 9 cm and the notch angle was 30°, the tensile strength was 37% less than that of the intact bi-material model, and at 90°, it was 15% less.

3. Numerical simulation

The numerical simulation of the laboratory test samples was performed using the 2D particle flow code (PFC2D), which is based on the versatile DEM. The explicit finite difference method (FDM) was adopted in PFC2D to solve the basic differential equations required for the problem solution. Several contact models are suggested for the simulation of geo-materials [49]. However, Potyondy and Cundall [50] proposed the parallel-bonded model (PBM), which includes the following characteristics: i) a relatively low ratio (3–7) of uniaxial to tensile strengths (UCS/TS), ii) linear strength increase due to confinement, and iii) the geo-material samples have a lower internal friction angle than laboratory specimens. Therefore, a flat-jointed model (FJM) was developed by Potyondy [45] to improve the PBM for jointed rocks. The FJM specifically enhances the UCS/TS ratio and provides a non-linear strength envelope for jointed specimens. A schematic of the FJM mathematical model is shown in Figure 11. The contact model contains a local contact surface with notional elements. These elements represent the contacting pieces in 2D models by lines of specific lengths and discs of specific area in 3D models. These notional grains create irregularities in the conventional regular particles and produce irregular polygons that represent the intrinsic structures as they exist in natural rocks [51]. This modeling scheme captures the strong interlocking interactions of different mineral grains and results in a macro-mechanical simulation that reasonably reflects real rocks.

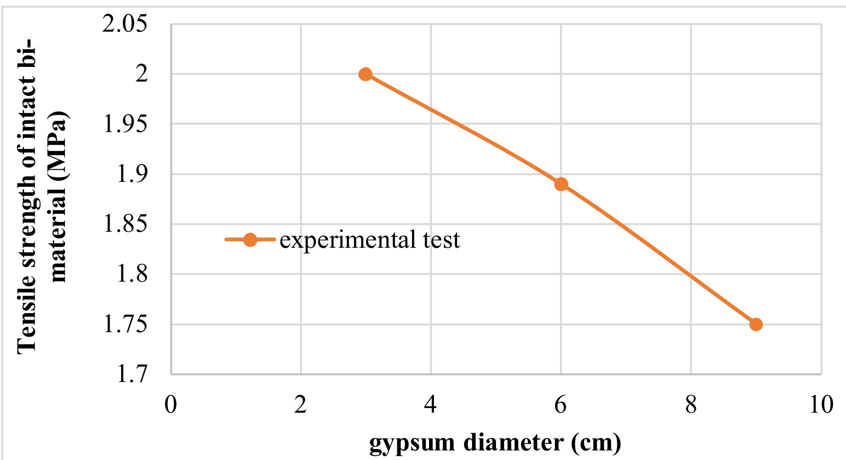

Figure 10. The variation of tensile strength of intact bi material model versus gypsum diameter.

3.1. Simulating Numerical Models with PFC2D and Software Calibration

The discrete element method (DEM) assembly for both gypsum and concrete materials was created according to the methodology outlined by Potyondy in his 2012 publication. This process involved a series of distinct steps, starting with the generation of individual particles to represent the material's granular structure. Following particle creation, these particles were packed together to form a cohesive assembly. An isotropic stress state was then applied to the packed assembly to ensure a stable initial configuration. Subsequently, any particles that were not properly connected and were effectively 'floating' within the assembly were identified and removed to improve the overall stability and representativeness of the model. Finally, a bonding mechanism was implemented between the particles to simulate the cohesive nature of gypsum and concrete.

In constructing the Discrete Element Model (DEM), the influence of gravity was considered negligible and subsequently ignored. This decision stemmed from the understanding that gravitational forces have a minimal effect on the macroscopic behavior and overall mechanical response of the simulated materials under the applied loading conditions .

The particle properties used in the DEM model, including parameters governing force-displacement behavior at contact points—specifically the Flat-Joint (FJ) contact model parameters—were carefully calibrated. This calibration relied on data from standard laboratory tests, namely uniaxial compression tests and Brazilian tensile strength tests, as detailed in Potyondy's (2012) work.

Through this calibration, the micro-mechanical behavior within the DEM model was directly linked to the experimentally observed macroscopic response of the materials. This iterative process involved adjusting micro-properties and conducting simulations until the results of the simulated uniaxial compression tests closely matched experimental data for both gypsum and concrete. This ensures that the DEM model accurately reflects the mechanical behavior of real-world materials.

For modeling and calibration, the particle micro-properties are defined as follows: both the concrete and gypsum models have a height of 108 mm and a width of 54 mm. The density of concrete is set at 3000 kg/m³, while that of gypsum is 2500 kg/m³. The minimum particle diameter for both models is 0.54 mm, and the maximum is 1.08 mm. The elastic modulus of contact (Ec) is 6 GPa for concrete and 1 GPa for gypsum. The standardized characteristics include a ratio of normal stiffness to shear stiffness (Kn/Ks) of 1.8 for concrete and 1.6 for gypsum, along with a gap ratio of 0.5 for both materials. The friction angles are set at 40° for concrete and 38° for gypsum.

According to the PFC user guide, a damping ratio of 0.7 was considered in the simulation to ensure quasi-static conditions.The Poisson's ratio was calibrated through the ratio of normal to shear stiffness. This ratio typically ranges from 1 to 3, where a value of 3 is selected for soft rocks and a value of 1 for hard rocks.

Tensile strengths are defined as 1 MPa for concrete (with a standard deviation of 0.25 MPa) and 0.1 MPa for gypsum (with a standard deviation of 0.1 MPa). Cohesion values are set at 22 MPa for concrete (standard deviation of 2.2 MPa) and 7.5 MPa for gypsum (standard deviation of 0.75 MPa). A total of two elements were used in the model for both concrete and gypsum specimens.

For the software calibration, the concrete samples utilized for the uniaxial compressive strength (UCS) test are shown in Figures 11a and 11b for the experimental and numerical data, respectively. Furthermore, Figures 11c and 11d present the experimental and numerical samples for the Brazilian Disc (BD) test. The results from both the experimental and numerical tests indicate a strong alignment.

Based on Table 1, it was observed that the modulus of elasticity (MOE), Poisson's ratio (υ), uniaxial compressive strength (UCS), and Brazilian Disc (BD) test were nearly equivalent to the values obtained through laboratory experiments.

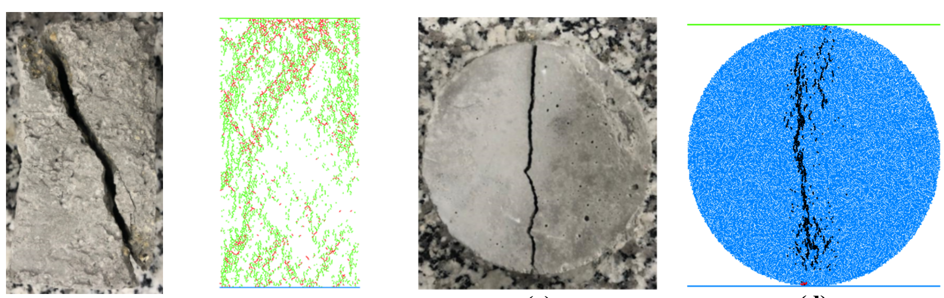

(a) (b) (c) (d)

Figure 11. Results of the failure mchanism model and crack propagation paths under uniaxial compression and Brazilian disk tests. (a) Laboratory-fractured specimen from the uniaxial compression test. (b) Numerical fractured model for the uniaxial compression test. (c) Laboratory-fractured specimen from the Brazilian test. (d) Numerical fractured model for the Brazilian test.

Table 1. Macromechanical Comparison of Concrete Samples from Laboratory Tests and Numerical Models

Material characteristics	Laboratory	PFC2D
MOE (GPa)	10	11
υ	0.11	0.1
UCS (MPa)	21	21.5
BD (MPa)	2.2	2.3

The UCS of gypsum samples was evaluated in the lab. These experiments were numerically simulated and compared in Figures 12a and 12b. The Brazilian Disc (BD) tests and their numerical simulations in PFC2D are also shown in Figures 12c and 12d.

For the calibration of the software, the gypsum samples utilized in the UCS test are shown in Figures 12a and 12b for the experimental and numerical data, respectively. Furthermore, Figures 12c and 12d present the experimental and numerical specimens for the Brazilian Disc (BD) test. The consistency observed between experimental measurements and numerical modeling outcomes confirms the close correspondence of the geomaterials' mechanical responses. For example, the numerical results for UCS, Young's modulus, and Poisson's ratio closely match those obtained in laboratory experiments, as illustrated in Table 2.

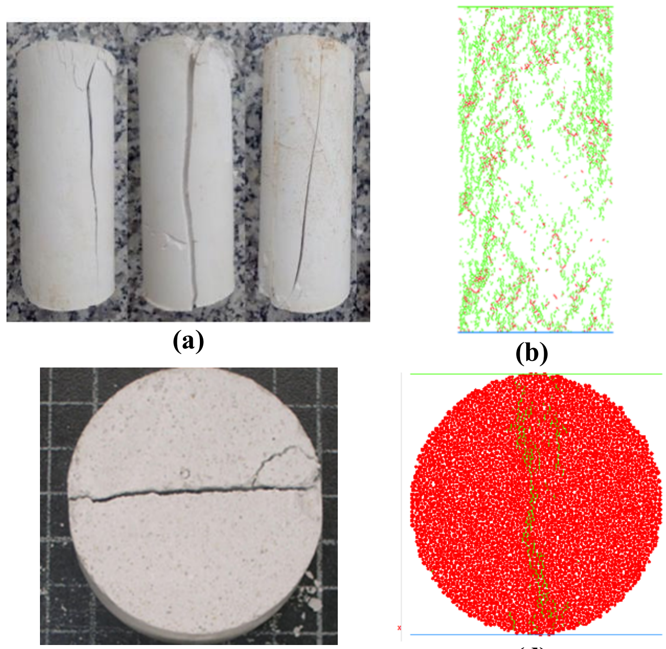

(a) (b) (c) (d)

Figure 11. Results of the failure mechanism model and crack propagation paths under uniaxial compression and Brazilian disk tests. (a) Laboratory-fractured specimen from the uniaxial compression test. (b) Numerical fractured model for the uniaxial compression test. (c) Laboratory-fractured specimen from the Brazilian test. (d) Numerical fractured model for the Brazilian test.

Table 2. Macro-mechanical properties for gypsum model vs. experiments.

Mechanical parameters	Lab-scale investigation results	Results obtained from PFC2D
MOE (GPa)	3	3.4
υ	0.15	0.16
UCS (MPa)	7.2	7.4
BD (MPa)	1	1.05

3.2. Numerical simulation of the bi-material disc containing an internal notch

Numerical axial tests for jointed bi-material discs were performed by creating a disc model in PFC2D (Figures 13–16). The PFC disc had a diameter of 12 cm. The sample consisted of 11,879 disks with a minimum radius of 0.27 mm. The model included two different materials: a gypsum core in the center and concrete around it. The gypsum diameter was 3 cm (Figure 13), 6 cm (Figure 14), and 9 cm (Figure 15), while the concrete thickness was 4.5 cm (Figure 13), 3 cm (Figure 14), and 1.5 cm (Figure 15). By removing bands of particles from the center of the model, a notch was created (Figures 13–15). The notch inclination varied from 0° to 90°, in steps of 15°. The pre-existing cracks were 1 mm wide. Additionally, three intact samples (without pre-existing cracks) were prepared (Figure 16). To study the effects of notch angle and bi-material thickness on failure mechanisms, twenty-four independent models were constructed. Axial compression was applied via the top and bottom boundaries, with the load monitored through reaction forces on the upper boundary.

The numerical modeling was carried out under plane strain conditions, which is appropriate for the specimen geometry and thickness considered in this .study

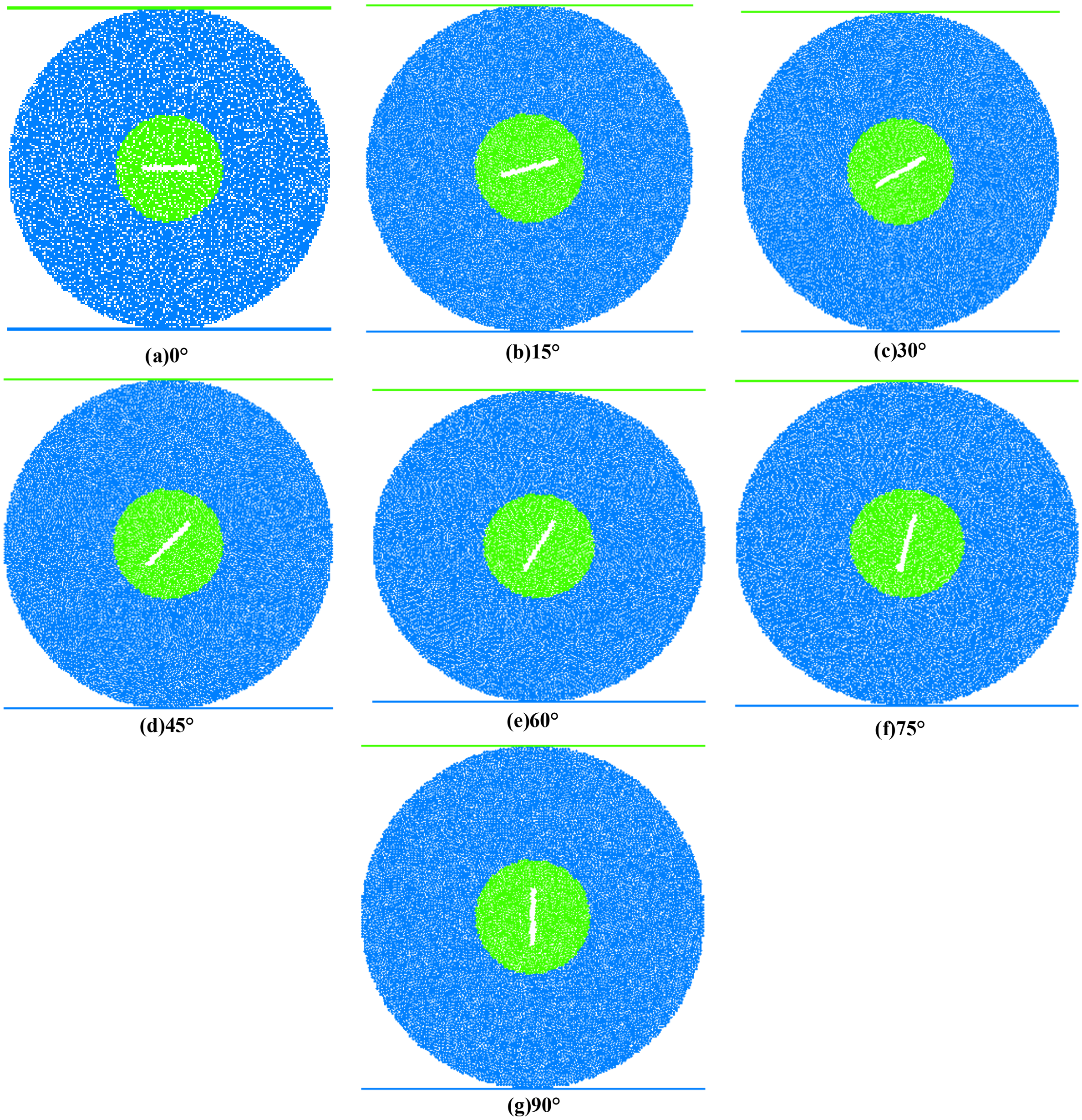

Figure 13. Numerical models featuring a central notch at different angles, with a gypsum diameter of 3 cm.

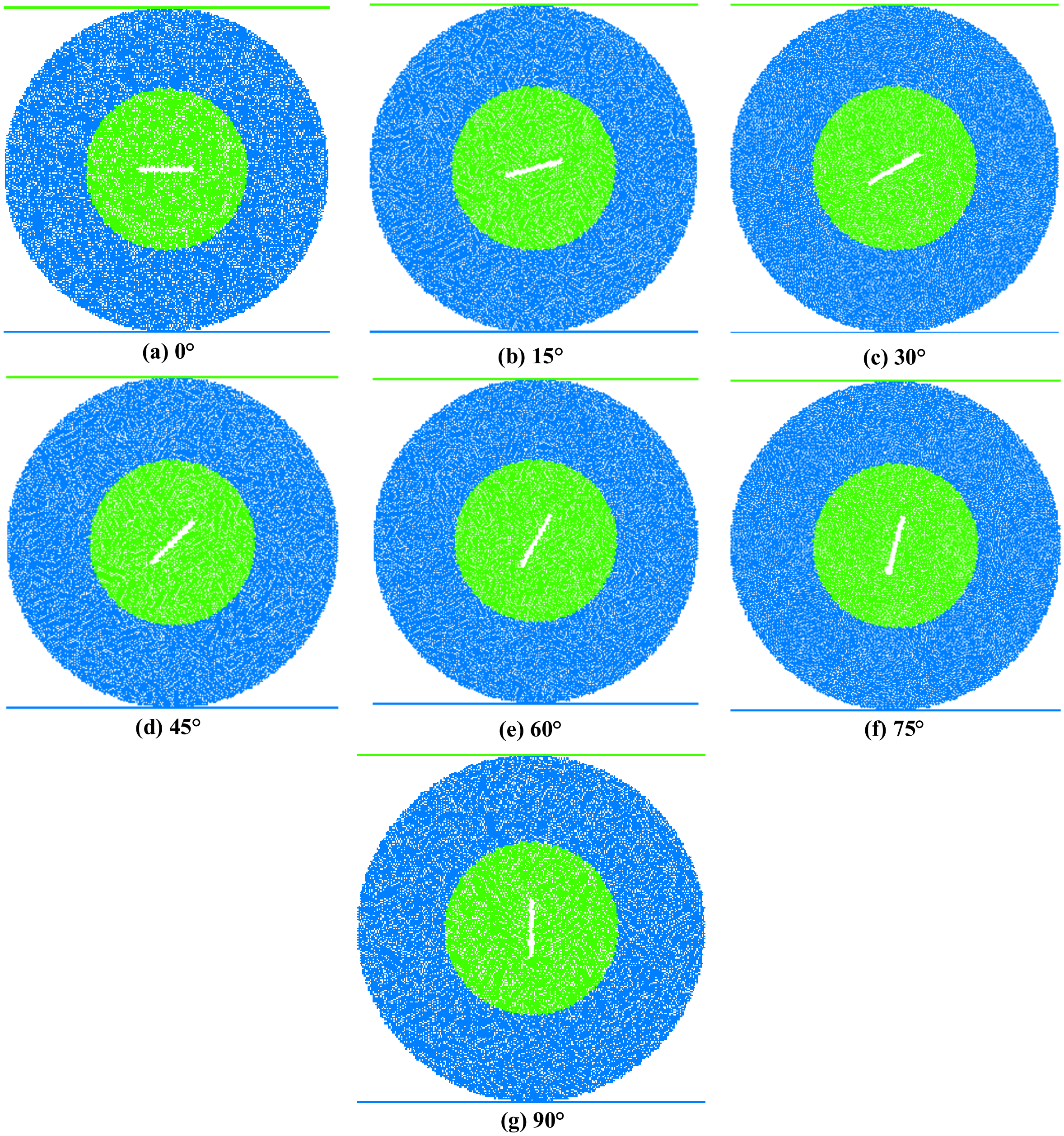

Figure 14. Numerical models featuring a central notch at different angles, with a gypsum diameter of 6 cm.

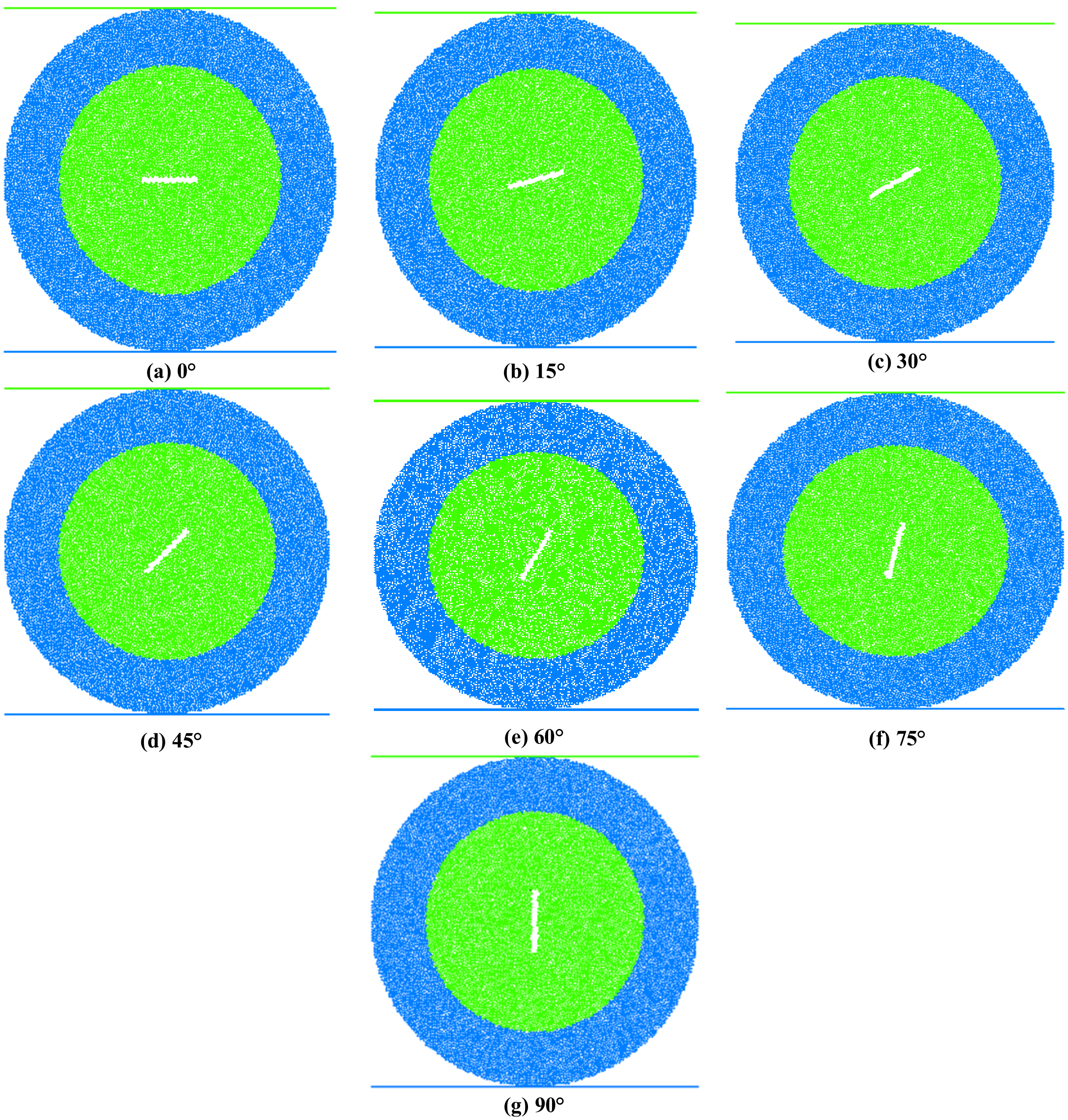

Figure 15. Numerical models featuring a central notch at different angles, with a gypsum diameter of 9 cm.

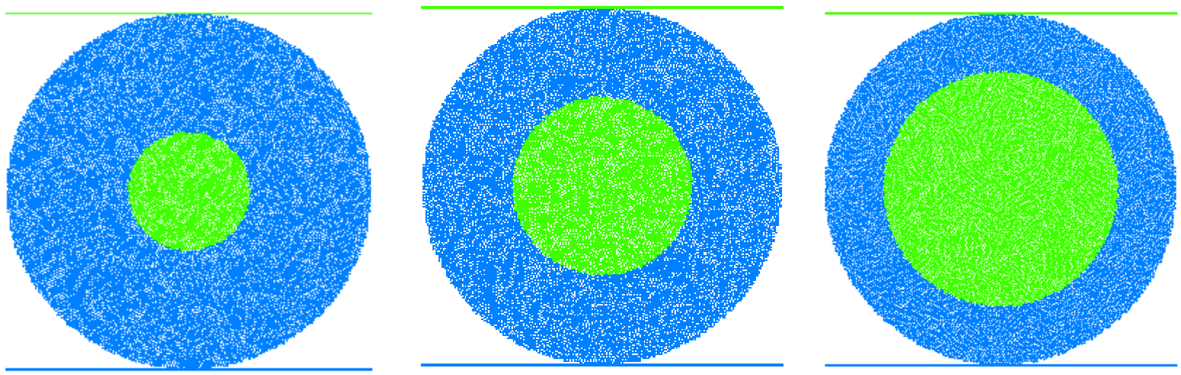

Figure 16. Numerical intact models (without pre-existing crack) with gypsum different diameters.

3.3. The simulated bond forces prior to the onset of crack propagation

The distribution of force vectors in between the particles of the assembly prior to the crack initiation is indicated in Figures 17–20. The black lines represent the compressive load vectors, while the red lines stand for the tensile forces. In samples where the angle of the notches exceeds 45 degrees, the highest concentration of tensile force occurs at the tip of the notches.

In contrast, for samples with a notch angle less than 45°, the maximum tensile force is observed at the walls of the notches.

Observations indicate that, in all specimens, the greatest compressive stress occurred at both the left and right sides of the two-material interfaces. Whereas the tensile strength of the material was less than its compressive strength, The tensile crack observed in these samples indicates that failure occurs mainly in areas experiencing maximum tensile force. In intact models, the tensile force was concentrated at the top and bottom of the bi-material interface, while the maximum compressive force was concentrated at the left and right sides of the bi-material interface (Fig 20). From Figure 17, it is evident that when the gypsum diameter is 30 mm, the distribution of tensile force is concentrated near the notch tip, while the compressive force is concentrated on the left and right sides of the notch. The compressive force is localized around the model and is distributed in a circular shape. As the notch angle increases, the position of tensile force concentration shifts from the notch wall to the notch tip. Regardless of the compressive force distribution, the tensile force remains confined to the notch area.

From Figure 18, its clear that when gypsum diameter was 60 mm, tensile force distribution was concentrated near the notch tip while compressive force was concentrated at the left side and right side of the notch. By comparison between Fig 17 and Fig 18, it is clear that in constant far field load, the values of both of the tensile force and compressive force was decreased by increasing the model dimension. The compressive force was concentrated non-locally and had distributed in a moon shape. The maximum tensile force concentration location shifted from the notch wall to the tip as the notch angle increased. Regardless of compressive force chain, tensile force was restricted to notch area.

As illustrated in Figure 19, when the gypsum layer measured 9 mm in diameter, the tensile stresses were focused near the notch tip, while the compressive stresses were primarily confined to the lateral regions of the notch. A comparison between Figures 17 and 19 shows that, with a constant far-field load, both tensile and compressive force values were found to decrease as the model dimensions increased. The compressive force was observed to have a non-local concentration, spreading in a narrow crescent shape. Furthermore, the location of maximum tensile force concentration was shifted from the notch wall to the tip with the increase in the notch angle. Despite the non-local characteristics of the compressive force, the tensile force was restricted to the notch area.

From Figure 20, it is apparent; that with the increasing model dimensions, both tensile and compressive force values were found to decrease under a constant far-field load. In the notch area, it was observed that the compressive force was generated non-locally, spreading in a thin crescent shape. In other words, the shape of the compressive force distribution was changed from a circular shape to a narrow crescent shape as the model dimensions increased. This alteration was found to significantly influence crack initiation stress and the path of crack growth.

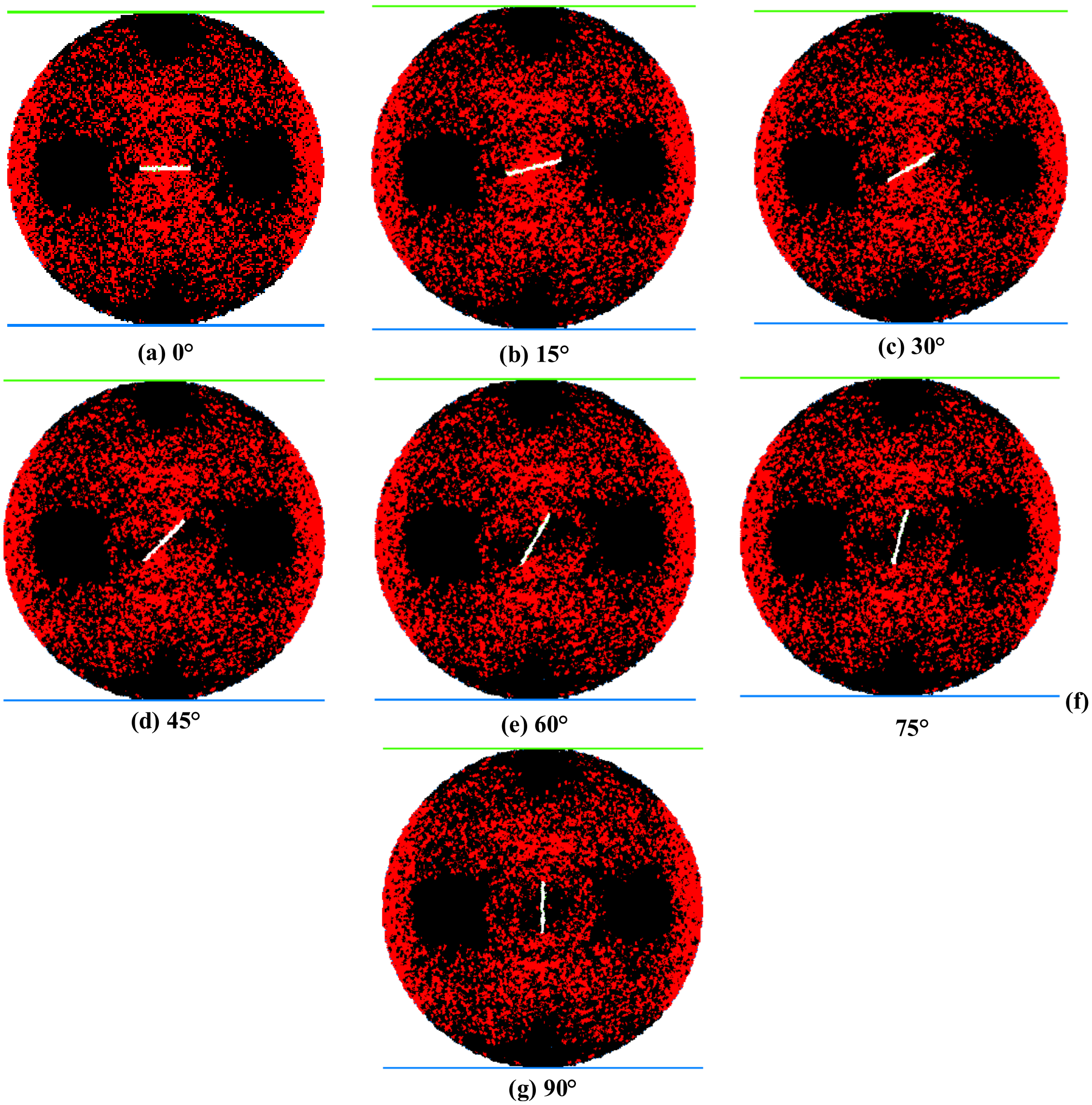

Figure 17. Distribution of bond forces in numerical models with a central notch at varying angles, using gypsum with a diameter of 3 cm.

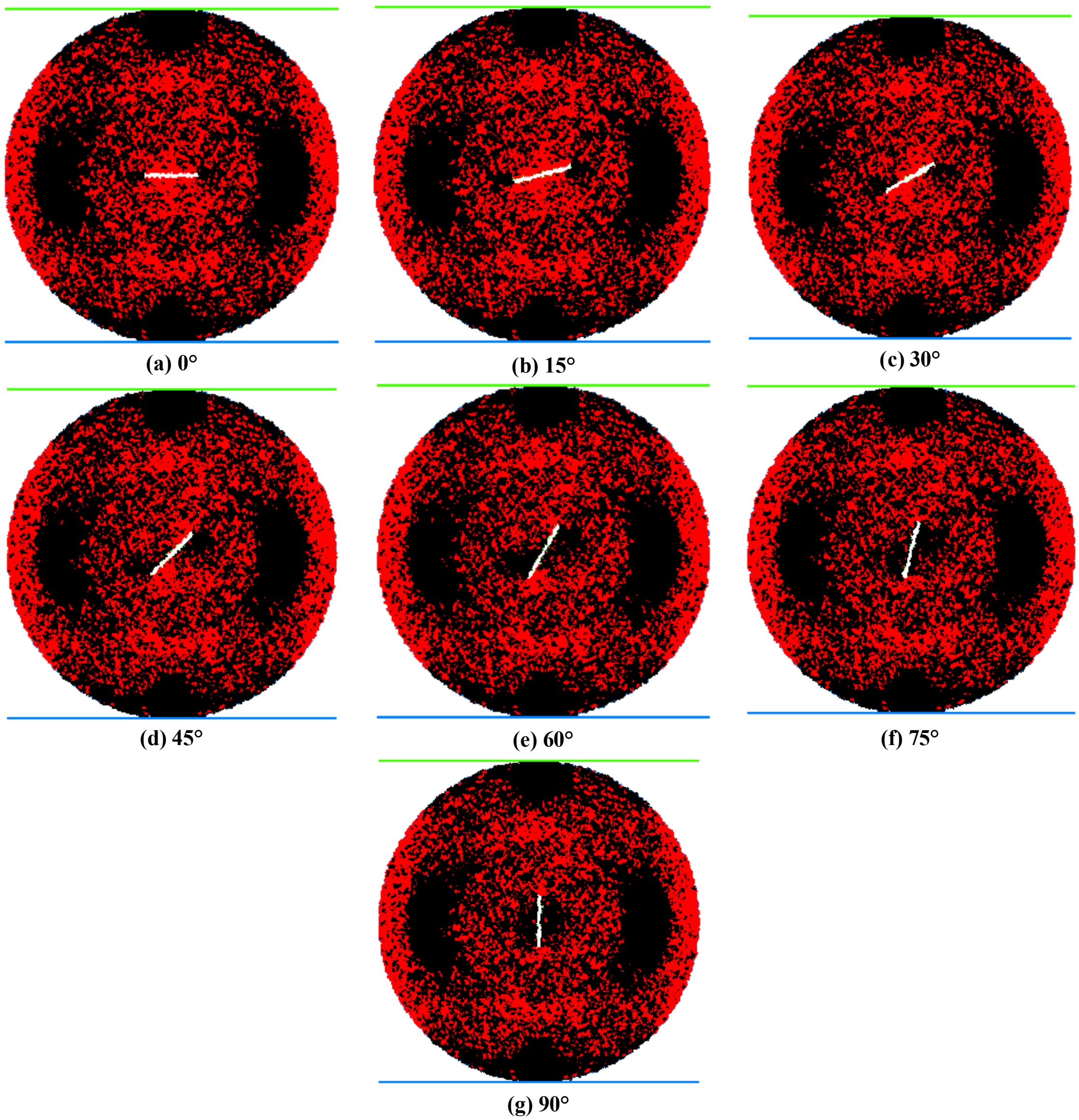

Figure 18. Distribution of bond forces in numerical models with a central notch at varying angles, using gypsum with a diameter of 6 cm.

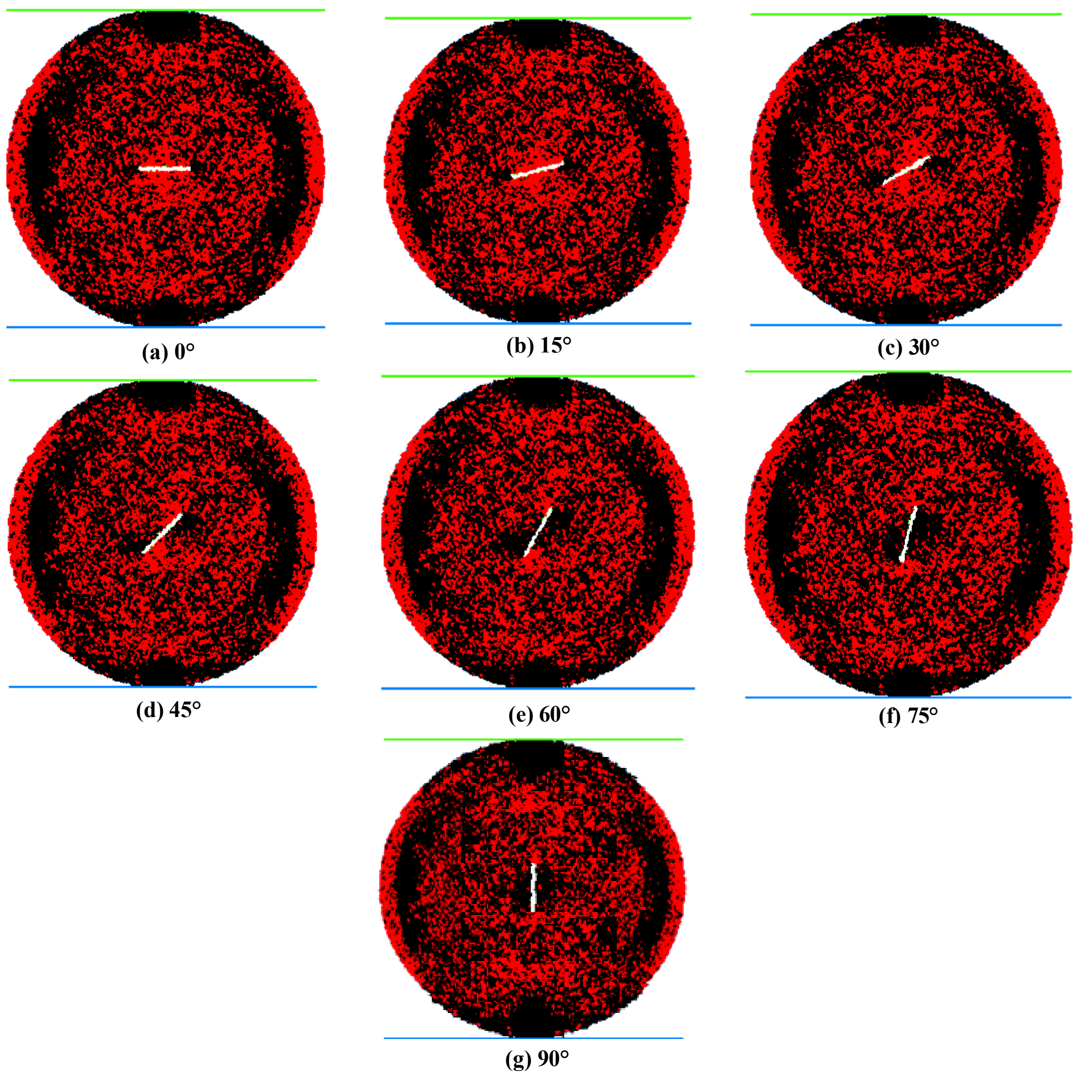

Figure 19. Distribution of bond forces in numerical models with a central notch at varying angles, using gypsum with a diameter of 9 cm.

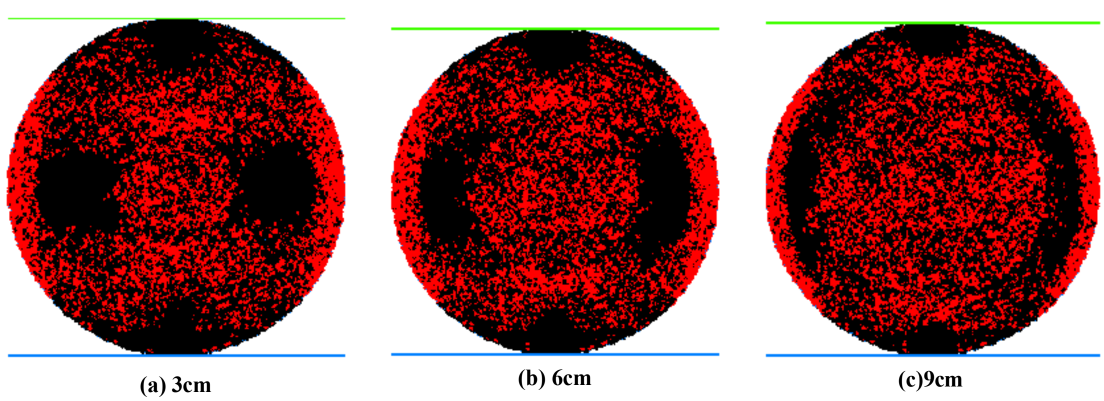

Figure 20. Distribution of bond forces in intact models with different gypsum diameters

3.4. Ross diagram of crack growth

Figures 21, 22, and 23 illustrate the rose diagrams of crack growth for model dimensions of 90 mm, 60 mm, and 30 mm, respectively. The micro-cracks in the modeled specimens occur at angles ranging from 75 to 105 degrees. The results indicate that the thickness of the specimens and the notch angles do not influence the direction of the major crack propagation path .

Figure 21 demonstrates that the number of tensile cracks reaches its maximum when the model dimension is 90 mm. As the model dimension decreases, the number of tensile cracks also decreases .

Additionally, the rose diagram for the intact model is shown in Figure 24. It reinforces the observation that the number of tensile cracks is highest at the 90 mm model dimension, with a reduction in the number of tensile cracks as the model dimension decreases.

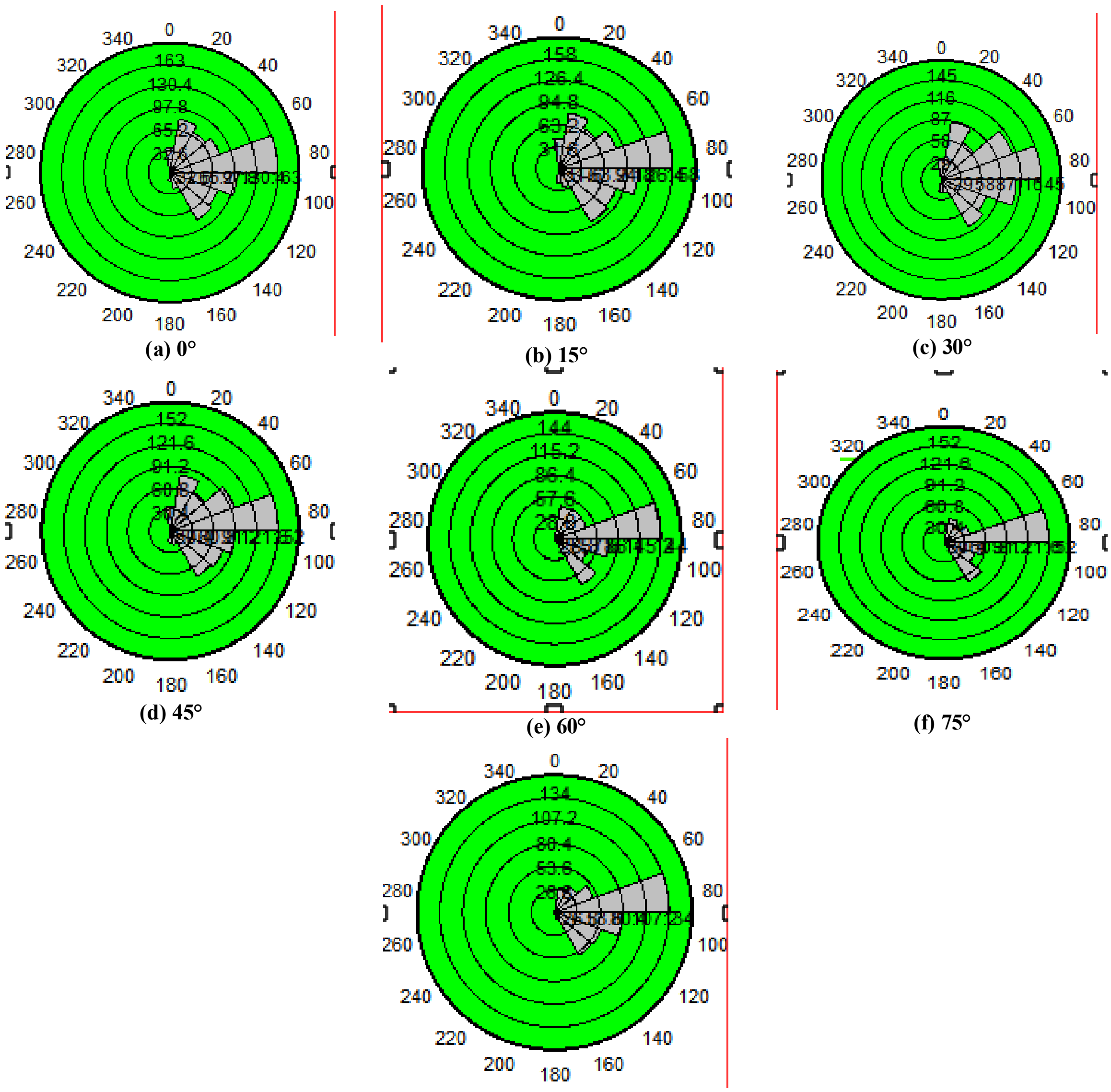

(a) 0° (b) 15° (c) 30° (d) 45° (e) 60° (f) 75° (g) 90

Figure 21. Ross diagram illustrating crack growth in numerical models featuring a central notch at various angles, with a gypsum diameter of 3 cm.

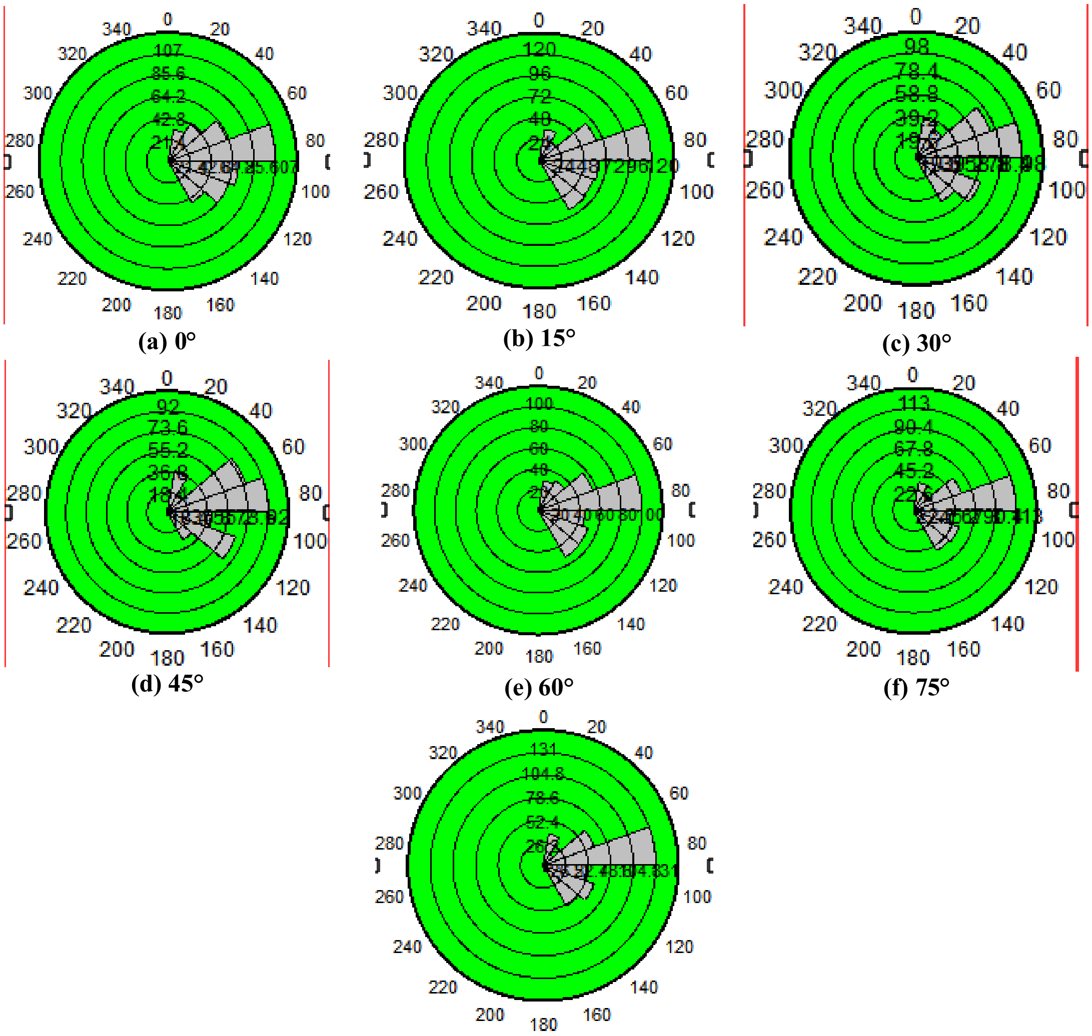

(a) 0° **(b) 15°** **(c) 30°**

(d) 45° **(e) 60°** **(f) 75°**

(g) 90°

Figure 22. Ross diagram illustrating crack growth in numerical models featuring a central notch at various angles, with a gypsum diameter of 6 cm.

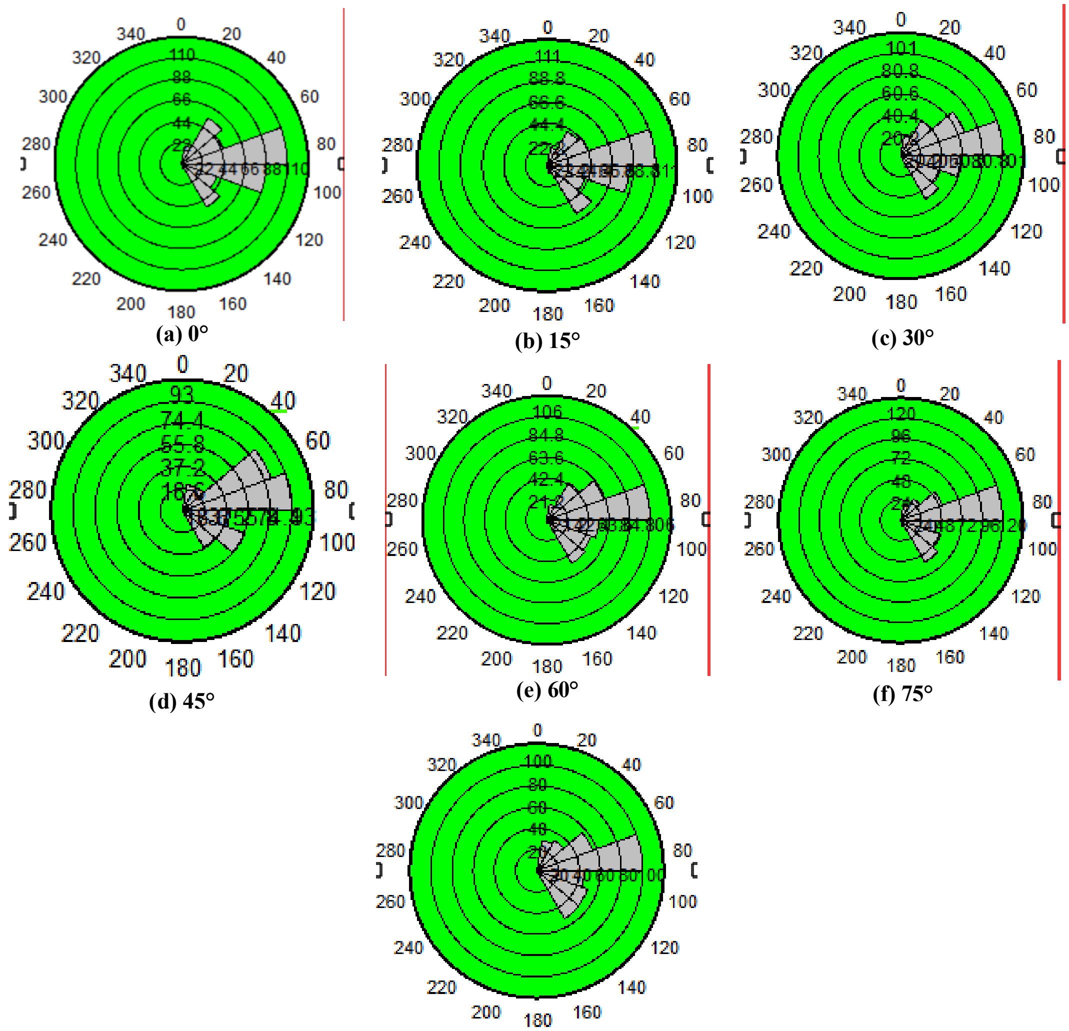

(a) 0° (b) 15° (c) 30° (d) 45° (e) 60° (f) 75° (g) 90°

Figure 23. Ross diagram illustrating crack growth in numerical models featuring a central notch at various angles, with a gypsum diameter of 9 cm.

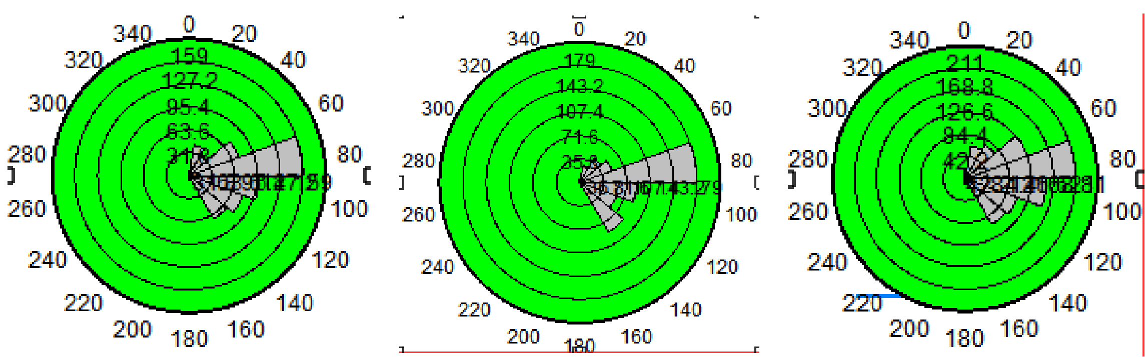

(a) 3cm (b) 6cm (c)9cm

Figure 24. Ross diagram illustrating crack growth in intact numerical models with different gypsum diameters

3.5. The crack growth patterns in the Brazilian discs

The tensile failure process in the pre-cracked Brazilian discs was recorded during the loading period, and the results are presented in Figures 25–28. The crack propagation paths observed in these tests revealed notable differences based on notch angle. When the notch angle exceeded 45° (as shown in Figures 25–27 d, e, f, and g), the tensile crack initiated from the notch tips and propagated parallel to the loading axis until it coalesced with the sample boundary. Conversely, when the notch angle was less than 45° (illustrated in Figures 25–27 a, b, and c), the tensile crack began at the notch walls and similarly propagated parallel to the loading axis until it reached the sample boundary. It is important to note that in the intact models, tensile cracks propagated through the material samples rather than along the predefined paths. Based on these findings, it can be concluded that the gypsum thickness does not significantly alter the overall crack growth path. However, the crack initiation position and crack intensity are affected by the specimen geometry. From Figure 25, it is evident that when the gypsum diameter was 30 mm, tensile cracks originated near the notch wall due to the distribution of tensile forces around the notch tip. As the notch angle increased, the concentration of tensile forces shifted from the notch walls to the notch tips. Additionally, the intensity of tensile cracks within the central core was greater than that in the outer cylinder, likely due to the brittleness of the central core.

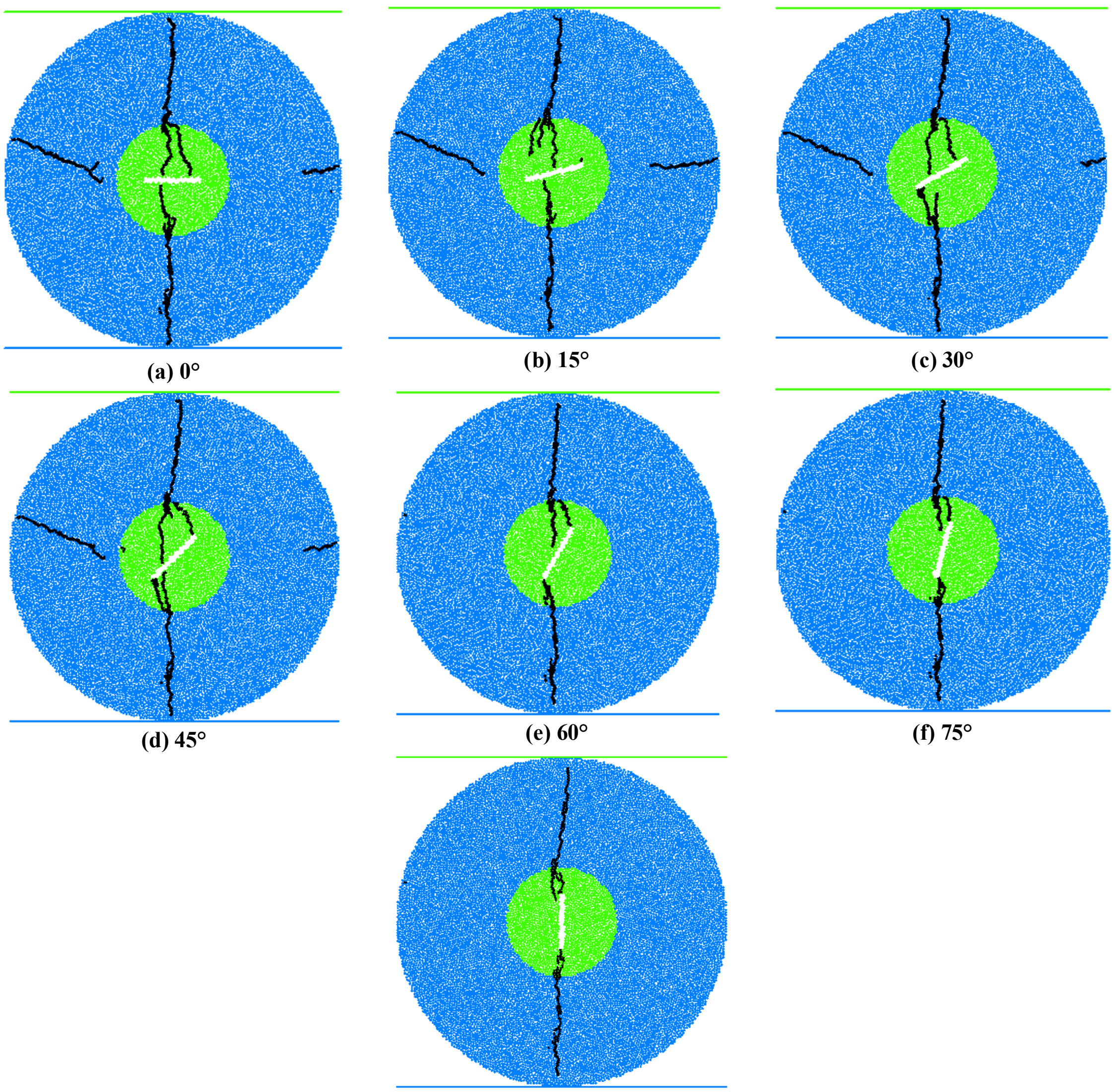

Figure. 25. Failure patterns in numerical models with a central notch at various angles, using a gypsum diameter of 3 cm.

As shown in Figure 26, when the gypsum diameter was 60 mm, tensile cracks began to form near the wall of the notch due to the distribution of tensile forces around the notch tip. As the angle of the notch increased, the concentration of tensile forces shifted from the notch wall to the notch tip.

Additionally, the intensity of the tensile cracks in the central core was greater than in the outer cylinder, likely due to the brittleness of the central core.

From Figure 27, it is clear that when the gypsum diameter was 90 mm, tensile cracks began to form near the notch wall due to the distribution of tensile forces near the notch tip. As the angle of the notch increased, the concentration of tensile forces shifted from the notch wall to the notch tip. The intensity of the tensile cracks in the central core was greater than in the outer cylinder due to the brittleness of the central core. By comparing Figures 27, 28, and 29, it is evident that the crack intensity increased with the larger diameter of the gypsum core.

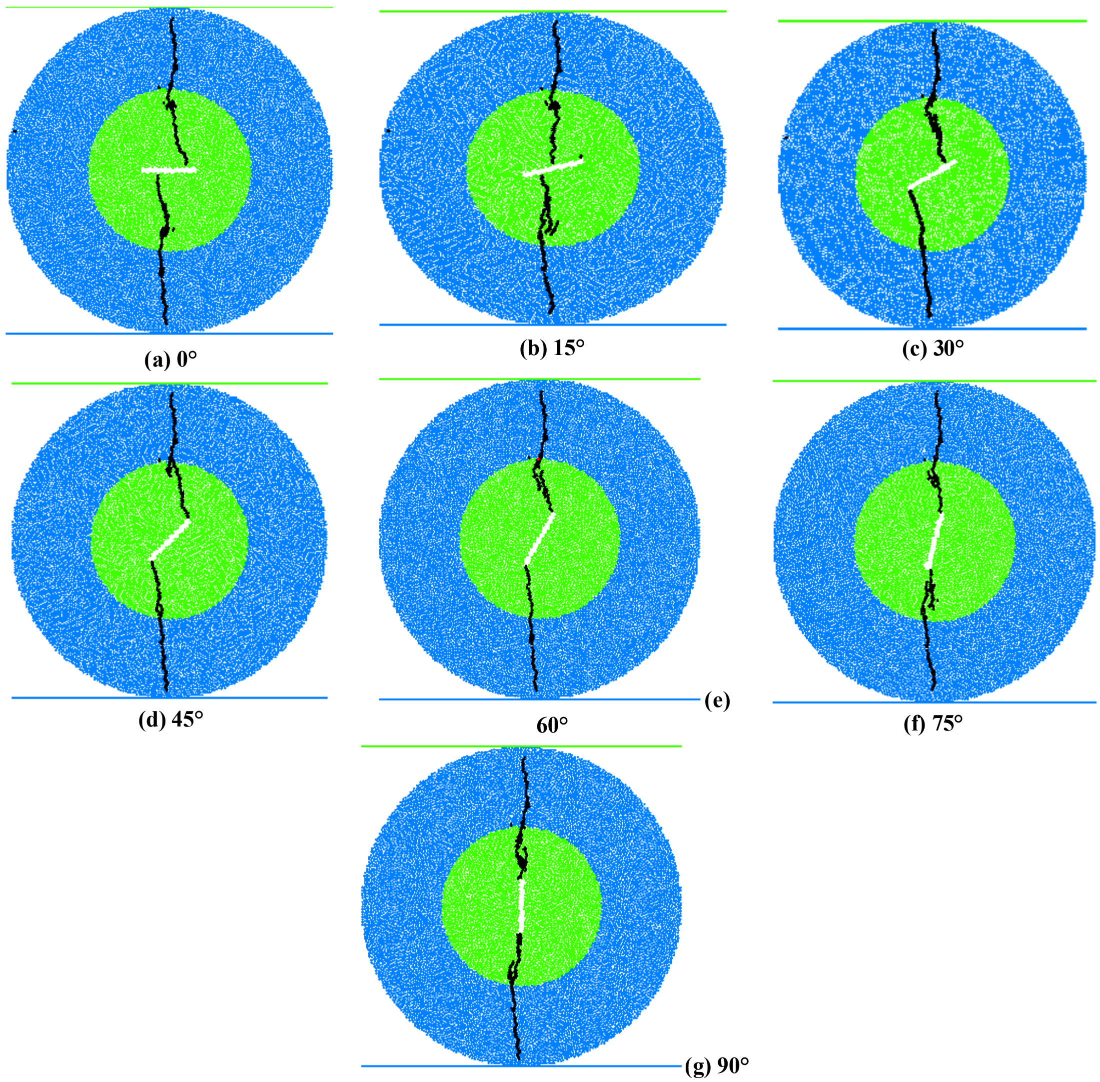

Figure 26. Failure patterns in numerical models with a central notch at various angles, using a gypsum diameter of 6 cm.

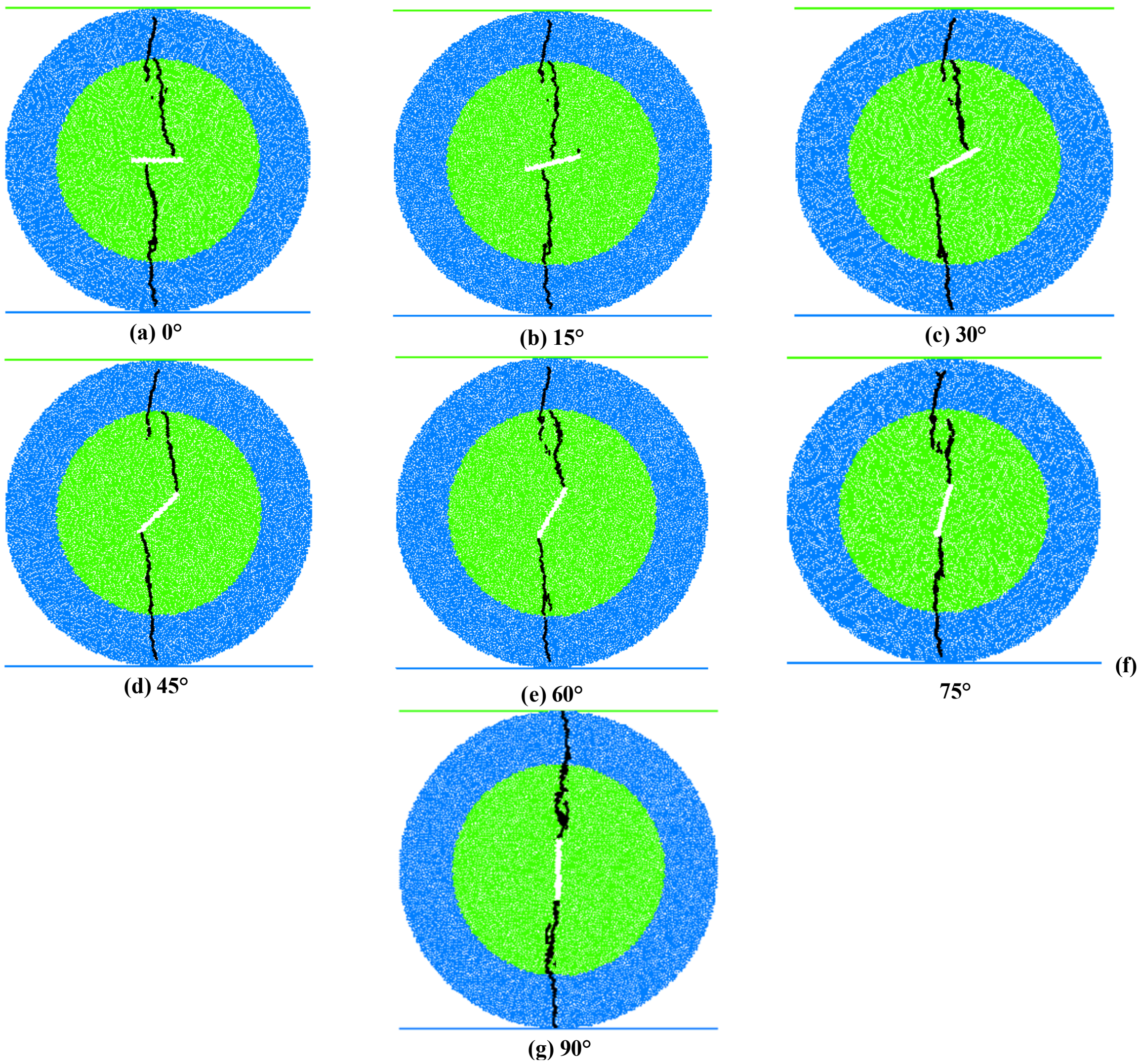

Figure 27: Failure patterns in numerical models with a central notch at various angles, using a gypsum diameter of 9 cm.

From Figure 28, the intensity of tensile crack in central core was more than outer cylinder due to brittleness effect of the central core. The crack intensity was increased by increasing the gypsum core diameter.

3.6. Investigation of Tensile Strength Characterization in the Numerical Model

Figure 29 depicts the tensile strength of bi-material notched discs featuring different configurations of notch angles. It can be observed that, for a fixed gypsum diameter, the tensile strength reaches its minimum value at a notch angle of 30° and its maximum value at 90°. Additionally, the tensile strength of the concrete specimen increases with greater thickness.

Comparing Figure 9 (Lab-Scale Investigation results) with Figure 29 (numerical results), it is evident that the tensile strength values obtained from both methods are very similar and align closely.

Figure 30 shows the tensile strength of intact bi-material discs with different gypsum diameters. By comparison between Figure 29 and Figure 30, it can be concluded that when the gypsum diameter was 3 cm and the notch angle was 30°, the tensile strength was 17% less than the intact bi-material model, while the tensile strength was 3% less than the intact bi-material model for a notch angle of 90°. When the gypsum diameter was 6 cm and the notch angle was 30°, the tensile strength was 28% less than the intact bi-material model, while the tensile strength was 9% less than the intact bi-material model for a notch angle of 90°. When the gypsum diameter was 9cm and the notch angle was 30°, the tensile strength was 41% less than the intact bi-material model, while the tensile strength was 17% less than the intact bi-material model for a notch angle of 90°.

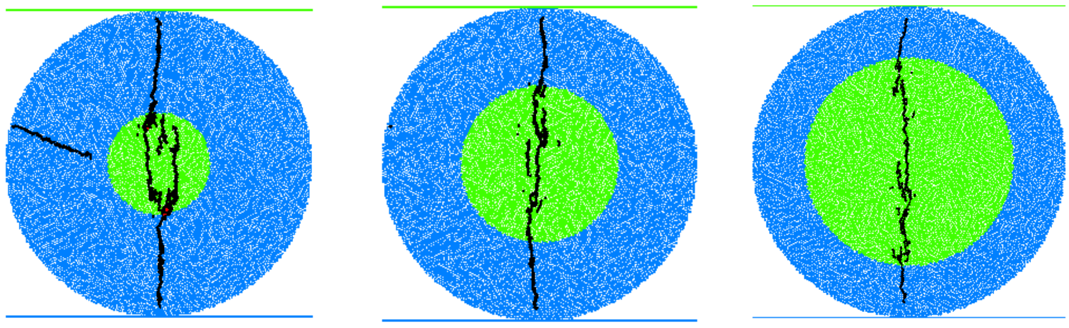

Figure 28. Failure patterns in numerical models of intact materials with varying gypsum diameters.

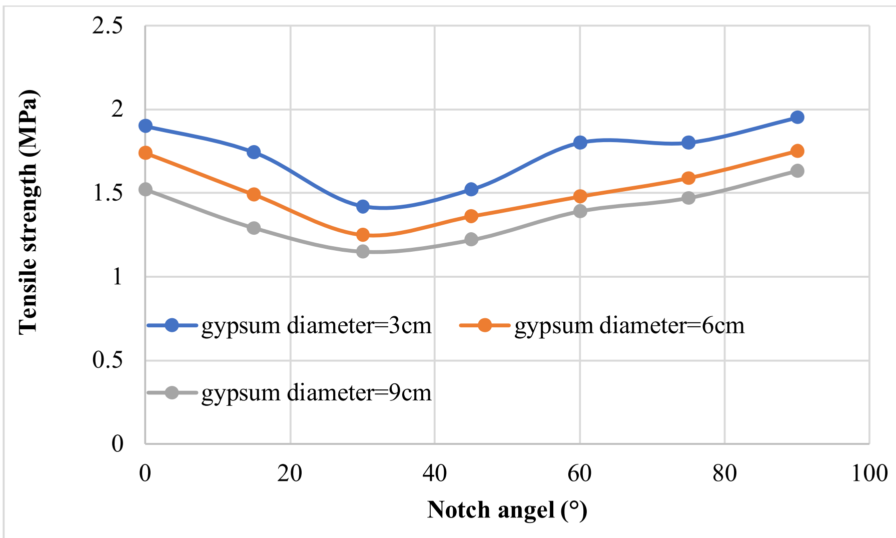

Figure 29. Variation of tensile strength versus notch angle for different gypsum diameters.

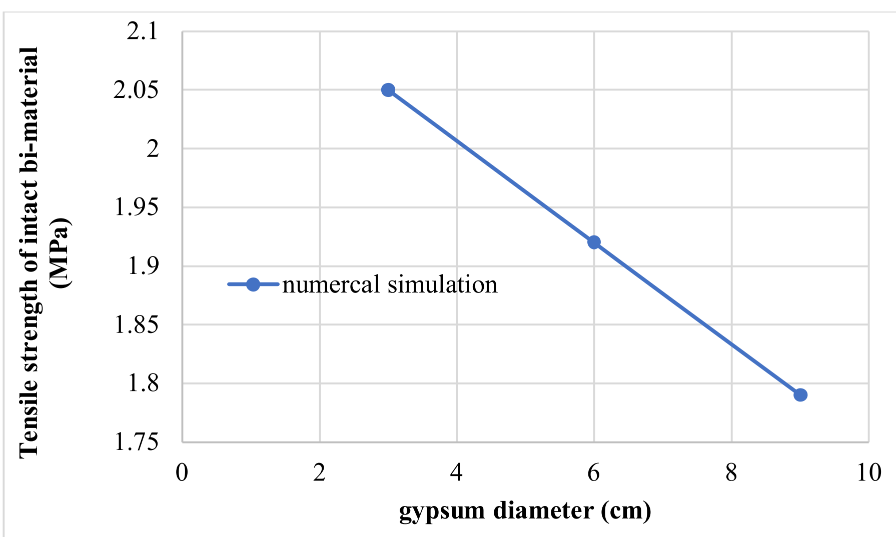

Figure 30. The variation of tensile strength of intact bi material model versus gypsum diameter.

4. Conclusions

This research explores the mechanical properties and tensile strength of brittle anisotropic materials through a combination of laboratory testing and PFC2D numerical modeling. Pre-cracked Brazilian discs were prepared and tested in the laboratory, and these tests were then simulated in PFC2D. The resulting tensile strengths and mechanical characteristics of the modeled geomaterial samples were analyzed and compared to the laboratory experimental results. Key findings are:

- Specimens with notch angles greater than 45° may begin to develop tensile cracks at the tips of the notches. These cracks can then propagate in the direction of the load until they reach the edges of the sample. Conversely, for angles less than 45°, cracks initiate at the walls of the notches and propagate in a similar manner. In intact models, tensile cracks propagate along the interface between the concrete and gypsum.
- Tensile strength of the concrete-gypsum specimen was minimized at a 30° notch angle and maximized at 90°, and it increased with concrete thickness.
- • The location of maximum tensile force was found to shift with notch orientation: it appeared at the notch tips when the angle exceeded 45°, but migrated to the notch walls at lower angles. By contrast, the highest compressive forces in gypsum–concrete specimens were always concentrated at the lateral regions of the bi-material interface.
- As deduced from the results shown in Figure 30, the microcrack angles ranged from 75 to 105 degrees across all models, independent of the notch angle and material thickness in the bi-material specimens.
- These numerical results corroborated well with the experimental findings.

Conflict of interest

The authors declare that they have no known competing financial interests or personal relationships that could have appeared to influence the work reported in this paper.

Data availability statement

The datasets generated during and/or analyzed during the current study are available from the corresponding author on reasonable request.

References

[1] Laubscher, D. H., & Jakubec, J. (2001). MRMR rock mass classification for jointed rock masses. In: Hustrulid, W. A., & Bullock, R. L. (Eds.), *Underground Mining Methods: Engineering Fundamentals and International Case Studies*, Society for Mining, Metallurgy and Exploration (SME), Englewood, CO, USA, pp. 474–481.

[2] Zhao, Z., Jing, L., & Neretnieks, I. (2012). Particle mechanics model for the effects of shear on solute retardation coefficient in rock fractures. *International Journal of Rock Mechanics and Mining Sciences*, 52, 92–102.

[3] Li, Y., Li, C., Zhang, L., Zhu, W., Li, S., & Liu, J. (2017). An experimental investigation on mechanical property and anchorage effect of bolted jointed rock mass. *Geosciences Journal*, 21, 253–265.

[4] Li, Y., Zhou, H., Dong, Z., Zhu, W., Li, S., & Wang, S. (2018). Numerical investigations on stability evaluation of a jointed rock slope during excavation using an optimized DDARF method. *Geomechanics and Engineering*, 14(3), 271–281.

[5] Alneasan, M., Behnia, M., & Bagherpour, R. (2019). Analytical and numerical investigations of dynamic crack propagation in brittle rocks under mixed mode loading. *Construction and Building Materials*, 222, 544–555.

[6] Li, Y., Wang, H., Cai, W., Li, S., & Zhang, Q. (2019). Stability monitoring of surrounding rock mass on a forked tunnel using both strain gauges and FBG sensors. *Measurement*, 153, 107449.

[7] Golewski, G. (2021). Validation of the favorable quantity of fly ash in concrete and analysis of crack propagation and its length using the crack tip tracking (CTT) method in fracture toughness examinations under Mode II through digital image correlation. *Construction and Building Materials*, 296, 122362.

[8] Wang, Y., Zhu, C., Song, Z. Y., & Gong, S. (2022). Macro-meso failure characteristics of circular cavity-contained granite under unconventional cyclic loads: A lab-scale testing. *Measurement*, 188, 110608.

[9] Wang, Y., Yang, H. N., Han, J. Q., & Zhu, C. (2022). Effect of rock bridge length on fracture and damage modelling in granite containing hole and fissures under cyclic uniaxial increasing-amplitude decreasing-frequency (CUIADF) loads. *International Journal of Fatigue*, 106741.

[10] Bahrani, N., & Kaiser, P. K. (2016). Numerical investigation of the influence of specimen size on the unconfined strength of defected rocks. *Computers and Geotechnics*, 77, 56–67.

[11] Benelfellah, A., Frachon, A., Gratton, M., Caliez, M., & Picart, D. (2014). Analytical and numerical comparison of discrete damage models with induced anisotropy. *Engineering Fracture Mechanics*, 121–122, 28–39.

[12] Yang, J., Chen, W., Yang, D., & Yuan, J. (2015). Numerical determination of strength and deformability of fractured rock mass by FEM modeling. *Computers and Geotechnics*, 64, 20–31.

[13] Hoek, E., Marinos, P., & Benissi, M. (1998). Applicability of the geological strength index (GSI) in

the Alps. *Bulletin of Engineering Geology and the Environment*, 57, 161–168.

[14] Barton, N. (2002). Some new Q-value correlations to assist in site characterisation and tunnel design. *International Journal of Rock Mechanics and Mining Sciences*, 39(2), 185–216.

[15] Zhang, L. (2010). Estimating the strength of jointed rock masses. *Rock Mechanics and Rock Engineering*, 43(4), 391–402.

[16] Gholami, R., Rasouli, V., & Alimoradi, A. (2012). Improved RMR rock mass classification using artificial intelligence algorithms. *Rock Mechanics and Rock Engineering*, 46(5), 1199–1209.

[17] Chen, C. S., Pan, E., & Amadei, B. (1998). Determination of deformability and tensile strength of anisotropic rock using Brazilian tests. *International Journal of Rock Mechanics and Mining Sciences*, 35(1), 43–61.

[18] Claesson, J., & Bohloli, B. (2002). Brazilian test: stress field and tensile strength of anisotropic rocks using an analytical solution. *International Journal of Rock Mechanics and Mining Sciences*, 39(8), 991–1004.

[19] Cai, M., & Kaiser, P. K. (2004). Numerical simulation of the Brazilian test and the tensile strength of anisotropic rocks and rocks with pre-existing cracks. *International Journal of Rock Mechanics and Mining Sciences*, 41(3), 450–451.

[20] Suo, Y., Chen, Z. X., & Rahman, S. (2018). Experimental and numerical investigation of fracture toughness of anisotropic shale rocks. In: *Proceedings of the 6th Unconventional Resources Technology Conference (URTeC)*, Houston, TX, USA.

[21] Yang, S. Q., & Huang, Y. H. (2014). Particle flow study on strength and mesomechanism of Brazilian splitting test for jointed rock mass. *Acta Mechanica Sinica*, 30(4), 547–558.

[22] Zhao, P., Xie, L., Fan, Z., Deng, L., & Liu, J. (2021). Mutual interference of layer plane and natural fracture in the failure behavior of shale and the mechanism investigation. *Petroleum Science*, 18(2), 618–640.

[23] Haeri, H., Shahriar, K., Marji, M. F., & Moarefvand, P. (2014). On the crack propagation analysis of rock-like Brazilian disc specimens containing cracks under compressive line loading. *Latin American Journal of Solids and Structures*, 11(8), 1400–1416.

[24] Haeri, H., Shahriar, K., Marji, M. F., & Moarefvand, P. (2014). Experimental and numerical study of crack propagation and coalescence in precracked rock-like disks. *International Journal of Rock Mechanics and Mining Sciences*, 67, 20–28.

[25] Tan, X., Konietzky, H., Frühwirt, T., & Dan, D. Q. (2015). Brazilian tests on transversely isotropic rocks: laboratory testing and numerical simulations. *Rock Mechanics and Rock Engineering*, 48(4), 1341–1351.

[26] Bidgoli, M. N., & Jing, L. (2014). Anisotropy of strength and deformability of fractured rocks. *Journal of Rock Mechanics and Geotechnical Engineering*, 6(2), 156–164.

[27] Bidgoli, M. N., & Jing, L. (2014). Effects of loading conditions on strength and deformability of fractured rocks–a numerical study. In: *Proceedings of EUROCK 2014 ISRM European Regional Symposium*, Taylor & Francis Group, Vigo, Spain, pp. 365–368.

[28] Li, Y., Zhou, H., Zhu, W., Li, S., & Liu, J. (2015). Numerical study on crack propagation in brittle jointed rock mass influenced by fracture water pressure. *Materials*, 8(6), 3364–3376.

[29] Li, Y., Wang, H., Zhu, W., Li, S., & Liu, J. (2015). Structural stability monitoring of a physical model test on an underground cavern group during deep excavations using FBG sensors. *Sensors*, 15(9), 21696–21709.

[30] Wang, Y., Li, X., & Zhang, B. (2016). Numerical modeling of variable fluid injection-rate modes on fracturing network evolution in naturally fractured formations. *Energies*, 9(6), 414.

[31] Wang, Y., Li, X., Hu, R., Ma, C., Zhao, Z., & Zhang, B. (2016). Numerical evaluation and optimization of multiple hydraulically fractured parameters using a flow-stress-damage coupled approach. *Energies*, 9(5), 325.

[32] Wang, Y., & Li, C. H. (2017). Investigation of the effect of cemented fractures on fracturing network propagation in model block with discrete orthogonal fractures. *Rock Mechanics and Rock Engineering*, 50, 1851–1862.

[33] Li, Y., Li, C., Zhang, L., Zhu, W., Li, S., & Liu, J. (2017). An experimental investigation on mechanical property and anchorage effect of bolted jointed rock mass. *Geosciences Journal*, 21, 253–265.

[34] Laghaei, M., Baghbanan, A., Hashemolhosseini, H., & Dehghanipoodeh, M. (2018). Numerical determination of deformability and strength of 3D fractured rock mass. *International Journal of Rock Mechanics and Mining Sciences*, 110, 246–256.

[35] Li, Y., Zhou, H., Dong, Z., Zhu, W., Li, S., & Wang, S. (2018). Numerical investigations on stability evaluation of a jointed rock slope during excavation using an optimized DDARF method. *Geomechanics and Engineering*, 14(3), 271–281.

[36] Wang, Y., Tan, W. H., Liu, D. Q., Hou, Z. Q., & Li, C. H. (2019). On anisotropic fracture evolution and energy mechanism during marble failure under uniaxial deformation. *Rock Mechanics and Rock Engineering*, 52, 3567–3583.

[37] Golewski, G. L. (2023a). Examination of water absorption of low volume fly ash concrete (LVFAC) under water immersion conditions. *Materials Research Express*, 10(8).

[38] Golewski, G. L. (2023b). Assessing of water absorption on concrete composites containing fly ash up to 30% in regards to structures completely immersed in water. *Case Studies in Construction Materials*, 9, e02337.

[39] Golewski, G. L. (2023c). Effect of coarse aggregate grading on mechanical parameters and fracture toughness of limestone concrete. *Infrastructures*, 8(8), 117

[40] Golewski, G. L. (2024). Enhancement fracture behavior of sustainable cementitious composites using synergy between fly ash (FA) and nanosilica (NS) in the assessment based on digital image processing procedure. *Theoretical and Applied Fracture Mechanics*, 131, 104442.

[41] Min, K. B., & Jing, L. (2003). Numerical determination of the equivalent elastic compliance tensor for fractured rock masses using the distinct element method. *International Journal of Rock Mechanics and Mining Sciences*, 40(6), 795–816.

[42] Wong, L. N. Y., & Einstein, H. H. (2009). Systematic evaluation of cracking behavior in specimens containing single flaws under uniaxial compression. *International Journal of Rock Mechanics and Mining Sciences*, 46(2), 239–249.

[43] Huang, D., Gu, D., Yang, C., Huang, R., & Fu, G. (2016). Investigation on mechanical behaviors of sandstone with two preexisting flaws under triaxial compression. *Rock Mechanics and Rock Engineering*, 49(2), 375–399.

[44] Sarfarazi, V., Haeri, H., Marji, M. F., & Zhu, Z. M. (2017). Fracture mechanism of Brazilian discs with multiple parallel notches using PFC2D. *Periodica Polytechnica Civil Engineering*, 61(4), 653–663.

[45] Potyondy, D. (2012). A flat-jointed bonded-particle material for hard rock. In: *Proceedings of the 46th U.S. Rock Mechanics/Geomechanics Symposium*, Chicago, IL, USA, pp. 1–10.

[46] Wu, S., & Xu, X. (2016). A study of three intrinsic problems of the classic discrete element method using flat-joint model. *Rock Mechanics and Rock Engineering*, 49(5), 1813–1830.

[47] Zhao, R., Lin, H., & Cao, P. (2018). Strength and failure characteristics of brittle jointed rock-like specimens under uniaxial compression: digital speckle technology and a particle mechanics approach. *International Journal of Mining Science and Technology*, 28(4), 669–677. https://doi.org/10.1016/j.ijmst.2018.02.002.

[48] Fan, X., Chen, R., Lin, H., Lai, H., Zhang, C., & Zhao, Q. (2018). Cracking and failure in rock specimen containing combined flaw and hole under uniaxial compression. *Advances in Civil Engineering*, 9818250.

[49] Cundall, P. A., & Strack, O. D. L. (1979). A discrete numerical model for granular assemblies. *Géotechnique*, 29(1), 47–65.

[50] Potyondy, D. O., & Cundall, P. A. (2004). A bonded-particle model for rock. *International Journal of Rock Mechanics and Mining Sciences*, 41(8), 1329–1364.

[51] Itasca. (2015). *PFC 5.0 Documentation*. Itasca Inc., Minneapolis, MN, USA.

انجمن مهندسی معدن ایران
نشریه مهندسی معدن و محیط زیست
نشانی نشریه: www.jme.shahroodut.ac.ir
دانشگاه صنعتی شاهرود

بررسی الگوهای گسترش ترک در مواد ناهمسانگرد در دیسک‌های شیاردار دوماده‌ای: بینش‌هایی از یک رویکرد ترکیبی آزمایشگاهی و عددی

وهاب سرفرازی[1]، هادی حائری[2]*، جین‌وی فو[3]، شادمان محمدی[1]، علیرضا شاکرو[4]

۱.گروه مهندسی معدن، دانشگاه صنعتی همدان، همدان، ایران
۲.گروه مهندسی معدن، مجتمع آموزش عالی زرند، دانشگاه شهید باهنر کرمان، کرمان، ایران
۳. دانشکده مهندسی عمران و حمل‌ونقل، دانشگاه منابع آب و نیروی برق شمال چین، ژنگژو ۴۵۰۰۴۶، چین
۴. گروه زمین‌شناسی، دانشکده علوم، دانشگاه شهید باهنر کرمان، کرمان، ایران

اطلاعات مقاله

تاریخ ارسال: ۲۰۲۵/۱۲/۲۲
تاریخ داوری: ۲۰۲۶/۰۴/۰۲
تاریخ پذیرش: ۲۰۲۶/۰۶/۲۶

DOI: 10.22044/jme.2026.17350.3438

کلمات کلیدی

ناهمسانگردی
ترک کششی
شیار
روش جریان ذرات (PFC)

چکیده

در این پژوهش، نمونه‌های دیسک شیاردار دوجنس ساخته و در آزمایشگاه مورد بررسی قرار گرفتند تا سازوکارهای شکست کششی غیرمستقیم آن‌ها ارزیابی شود. برای تعیین خواص مکانیکی نمونه‌ها، آزمایش‌های مقاومت کششی برزیلی تحت نرخ بارگذاری ۰/۰۱۶ میلی‌متر بر ثانیه انجام شد. نمونه‌های دیسکی دارای یک شیار مرکزی بوده و از ترکیب دو ماده شامل بتن و گچ تشکیل شدند. در این نمونه‌ها، گچ به‌عنوان ماده اول در بخش مرکزی (هسته) قرار گرفت، در حالی‌که بتن به‌عنوان ماده دوم، ناحیه پیرامونی به شکل یک حلقه در اطراف هسته مرکزی را تشکیل داد. به‌منظور بررسی تأثیر پارامترهای هندسی، قطر هسته مرکزی و ضخامت حلقه پیرامونی به‌عنوان متغیرهای طراحی در نظر گرفته شدند. در مجموع، ۲۱ نمونه آماده‌سازی شده و تحت بارگذاری محوری مورد آزمایش قرار گرفتند. همچنین، برای تحلیل دقیق‌تر فرآیند شکست و اعتبارسنجی نتایج آزمایشگاهی، شبیه‌سازی عددی آزمایش‌ها با استفاده از روش جریان ذرات انجام شد. نتایج آزمایشگاهی نشان داد که ابعاد شیار و نوع مواد تشکیل‌دهنده نمونه‌ها تأثیر قابل‌توجهی بر رفتار مکانیکی و ویژگی‌های شکست نمونه‌های ناهمسانگرد دارند. تغییر در هندسه شیار و ترکیب مواد موجب تغییر در نحوه تمرکز تنش، محل آغاز ترک و مسیر انتشار آن شد. علاوه بر این، مقایسه نتایج حاصل از آزمایش‌های آزمایشگاهی و مدل‌سازی عددی، تطابق بسیار خوبی را در زمینه رشد و گسترش ترک‌ها نشان داد که بیانگر توانایی روش جریان ذرات در پیش‌بینی رفتار شکست این نوع نمونه‌ها است. علاوه بر این، بررسی جامع رفتار نمونه‌ها از طریق مدل‌سازی عددی شامل تحلیل توزیع نیروهای پیوندی، رزدیاگرام‌ها و الگوهای رشد و گسترش ترک‌ها انجام شد. نتایج این تحلیل‌ها امکان بررسی دقیق‌تر فرآیند انتقال تنش، نحوه شکست در فصل مشترک دو ماده و تأثیر متقابل هسته مرکزی و ناحیه پیرامونی بر رفتار شکست نمونه‌های دوجنس را فراهم نمود.

✉ **نویسنده مسئول مکاتبات**: hadihaeri@uk.ac.ir (ه. حائری)